CHALMERS
UNIVERSITY OF TECHNOLOGY

Modeling of diesel particulate filter (DPF)

Master's thesis in Automotive Engineering

Obadah Almasri

Department of Mechanics and Maritime Sciences

CHALMERS UNIVERSITY OF TECHNOLOGY

Gothenburg, Sweden 2022

www.chalmers.se

Master's thesis in Automotive Engineering

Modeling of diesel particulate filter (DPF)

Obadah Almasri

CHALMERS
UNIVERSITY OF TECHNOLOGY

Department of Mechanics and Maritime Sciences

CHALMERS UNIVERSITY OF TECHNOLOGY

Gothenburg, Sweden 2022

Modeling of diesel particulate filter (DPF)

Obadah. Almasri

Examiner: Jonas Sjöblom, Mechanics and Maritime Sciences

Master's Thesis 2022

Department of Mechanics and Maritime Sciences

Chalmers University of Technology

SE-412 96 Göteborg

Sweden

Telephone + 46 (0)31-772 1000

Cover: Exhaust after-treatment system for Volvo D13 engine.[1]

Abstract

Diesel engines using are still expected, especially for inland and sea transport. Recently, legislation in the European Union has been tightened to reduce emissions from diesel engines and increase fuel efficiency. To meet these needs, an exhaust system must be developed. The diesel particulate filter (DPF) is the part responsible in the exhaust system for purifying most of the soot particles harmful to humans and the environment.

This project aims to study the effect of pressure drop on soot loading, where the pressure drop rises with the steadily increasing amount of soot. Therefore, the attempt to influence the pressure drop helps improve the efficiency of soot filtration inside the DPF. The software used was ***Axisuite,*** a commercial program developed by ***Exothermia*** to study the exhaust system of diesel engines, where the model was created entirely identical in terms of dimensions and the type of materials with what was used in the experiment.

The engine Volvo HD D13 was used during the experiment to collect data. The experiment data was collected during custom-made test cycle to understand soot formation and its effect on pressure drop under different engine working conditions. The main parameters that have been checked for influence on the pressure drop are wall permeability, diffusion mechanism correction factor, interception mechanism correction factor, and soot reaction speed inside the diesel particle filter to better agree with the experimental data. The results from the model show that the pressure drop is significantly improved with the experimental data and thus its effect on soot loading. The model also allows comparing sure reduction when using the same porosity-permeability wall and a different permeability.

Keywords: Diesel particulate filter, Axisuite, Parameter estimation, Diesel oxidation catalyst.

Acknowledgments

I want to extend my sincere thanks and gratitude to the examiner Jonas Sjöblom for the tremendous support he provided during the project, especially regarding the chemical aspect, and for his insight into analyzing the results. Thanks to the laboratory supervisor, Andreas Mattson, for assisting him during the experiments. I would also like to thank the *Exothermia* team for their support during the project. I want to thank everyone who has supported and helped me during this thesis.

Obadah Almasri, Gothenburg, June 2022

Contents

1. Introduction

This section explains the background of the master's thesis and defines the objective of this project and the desired results. In addition, an explanation of the method used to reach the project's goal and the limitations.

1.1 Background

At present, the use of diesel engines is still widespread. Diesel engines are widely used in land transport operations, in giant cargo ships, and in heavy equipment used in construction operations, which requires a large amount of energy due to the efficiency of diesel engines and their ability to generate the necessary power and relatively low fuel consumption, so diesel engines are the best choice. In contrast to these significant advantages of diesel engines, there is a dark side.[2] Diesel engines are one of the essential sources responsible for hazardous emissions that pose a significant danger to human health and the environment.

Fossil fuels contain latent chemical energy. To obtain this energy and convert it into kinetic energy, diesel engines use the principle of auto-ignition, where air and fuel are mixed inside the combustion chamber at high-temperature degrees. That helps to convert the chemical energy to kinetic energy.

In the case of perfect combustion, carbon and oxygen are completely burned without generating any other harmful element. However, this chemical equilibrium state is difficult to verify for several reasons, including changes in temperature and the lack of mixing of the elements well due to the short time [3]. Thus, the incomplete combustion of carbon and hydrogen leads to the formation of several harmful elements: Particulate matter. This component makes up about half percent of the exhaust diesel engine [4].

Nitrogen oxides and particles are the most important sources of air pollution present, which lead to dangerous consequences for human health and the environment at the same time. [5]The particle matter is one of the most important causes of asthma and heart disease because of its negative impact on air quality.

There are two types of particle matter, $PM_{2,5}, PM_{10}$ where the $PM_{2,5}$ residues from the combustion of fossil fuels, the PM_{10}, resulting from tire friction with the road, and brakes. Because of the danger of nitrogen oxides and PM to human health and the environment, the European Union imposes strict laws regarding emissions from combustion engines, especially diesel engines, to reduce emissions; by looking at table 1 below, can be seen the development in reducing the number of emissions over time, especially NO_X and PM [6].

Table 1 : EU emission standard for heavy-duty diesel engine[7].

Date	CO (g/kWh)	HC(g/kWh)	NOx(g/kWh)	PM(g/kWh)
1992	4.5	1.1	8	0.612
2021	2	0.22	0.60	0.016

The technology behind reducing emissions is using different technology for different elements. The NO_X emission can be reduced by using the EGR. It is a technology-based on recycling the exhaust gas into the combustion chamber and mixing it with the air entering the combustion chamber, which leads to a concentration decrease of oxygen inside the combustion chamber and a decrease in temperature.[8] But the low-temperature forms of Particle matter and CO and HC mean the need for other treatment systems.

The diesel oxidation catalyst (DOC) technology can oxidize CO and HC and convert these elements to CO_2 and H_2O. When the elements mentioned above (CO, HC) are reduced using the DOC, the exhaust gas still contains harmful elements like NO, NO_2, and PM. To reduce these elements, the DPF system should be used where the system will filter out the Particular matter. The rest of the elements, NO_2 and NO, can be reduced where the SCR covert the NO_X to N_2 and H_2O [9]. After reducing the NOX through SCR, there is an amount of ammonia that is not used during this process. To treat this quantity of ammonia, the ASC system will be used to oxidize the ammonia into CO_2, H_2O, N_2.

Figure 1 presents a design for an after-treatment system for a diesel engine. The figure also shows the elements entering at the beginning of the system and the elements leaving after going through the different filtering stages. This research will focus on DPF technology to understand how it works and the chemical reactions inside it, and how to influence this different element.

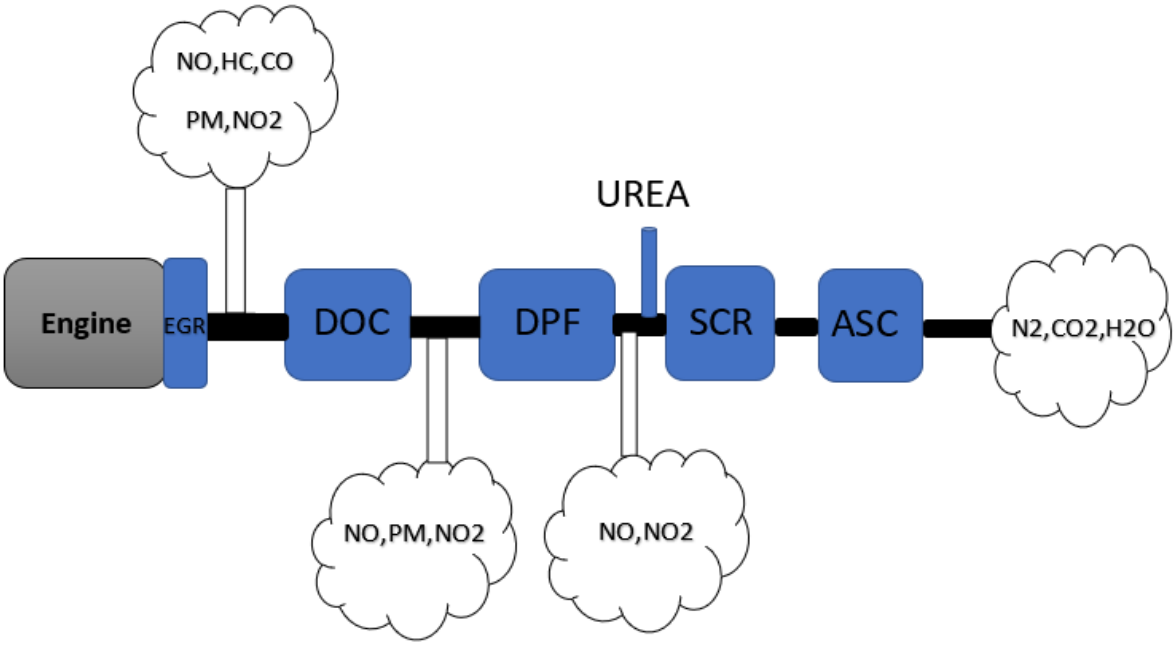

Figure 1: Aftertreatment System for diesel engine

1.2 Purpose

The objective of this master's thesis is to evaluate the data previously collected from an HD diesel engine, some used in Volvo Trucks equipped with a DPF, by studying and analyzing the data using the Axisuite software. During this project, work will also enhance and develop the current model by improving the input data and conducting additional experiments to obtain the best results.

1.3 Limitations

From the master's thesis description, many limitations will be considered and will be mentioned in this chapter to obtain the best results. The data has already been collected from the HD diesel engine Volvo D13, and no data will be taken from other engines. The focus of this master thesis will be on diesel particulate filter DPF only, and the other parts in filter systems like SCR and ASC will not be taken into consideration. No custom DPF design will be used for this project, so design aspects will not be considered.

1.4 Research questions

Based on the background and purpose of the project, many questions can be asked in this project. In this case, the following questions will be answered.

RQ1: How to create a workflow for simulation of a DPF by using Axisuite?

RQ2: How can Axisuite software optimize the previous model of pressure drop affecting feeding soot?

1.5 Effects of particulate matter

In this section, the impact of particulate matter on human health and the environment will be discussed, as well as the difference in the number of emissions in Sweden over time.

1.5.1 Particulate Matter Effect on Environment

Carbon dioxide is one of the most important sources of pollution responsible for global warming at present, as fuel burning is one of the causes of an increase in the amount of carbon dioxide in the air because of the combustion process, where the carbon in the components of fossil fuels combines with the oxygen carried with the air entering the combustion chamber to form carbon dioxide.[10] With the passage of time and the increasing use of combustion engines, large amounts of carbon dioxide were released into the air; these gases are greenhouse gases as they absorb heat and release it over time, and the steady increase in the amount of these gases leads to an increase in the amount of energy emitted from them and thus a rise in the Earth's temperature, or the so-called global warming. [10]

Recently, severe climatic changes have appeared, including the rise in global temperature and its adverse effects. The risks are not limited to global warming, as there are local emissions sources that lead to high risks to human health and the environment at the same time. They have a high risk to human health, and air pollution is considered one of humanity's most critical current risks because of its severe consequences[11]. The emission of harmful particles from various sources (vehicles, transport) is one of the causes of atmospheric pollution and its severe implications for human health.

There is an effect of particles on global warming, as the particles scattered in the air interact with solar radiation, which leads to a decrease in visibility in the surrounding atmosphere. The size of the particles and the method of interaction have a significant role in how they affect the atmosphere, as they can lead to an increase in temperature (global warming) or lead to freezing. [12]

1.5.2 Particulate Matter Effect on Human Health

The impact of particulate matter on human health is no less dangerous than its impact on the environment, as research has proven that the air contaminated with particulate matter ($PM_{2,5}, PM_{10}$) is one of the most important causes of several serious health problems: Respiratory problems, blockage of blood vessels, which lead to heart attacks, in addition to tissue damage, vision and cancer[11] .Studies show the adverse effects on people's health who live in cities with a high level of air pollution compared to less polluted cities where the most vulnerable population groups are children, pregnant women, and the elderly.

According to the World Health Organization, air pollution from particulate emissions leads to approximately 4.2 million deaths per year, and the danger of these particles is possible in their small size. The person does not feel symptoms directly when caught, and most of the symptoms are long-term, leading to severe diseases, as mentioned above.[13]

1.5.3 Reducing of Particulate Matter Emissions

With the increase in the proportion of harmful emissions into the atmosphere, work began on measures to reduce emissions from diesel engines, especially as the European Union imposed over time strict standards to reduce emissions of harmful particles into the atmosphere, the latest of which was Euro VI, and this strategy succeeded in reducing emissions significantly, as is evident in Table 1 in the first section [14]. With the start of the use and development of various filtering systems to reduce toxic emissions, studies showed an apparent reduction in atmospheric pollution of harmful particles.

Figures 2,3 shows the difference in the concentration of particulate emission ($PM_{2,5}, PM_{10}. NO_X$) in the atmosphere issued from different sources in Sweden between 1999 and 2020. It can be seen clearly that the percentage of emissions issued by transport (Light Blue) decreased significantly for NO_X from 162 [kton] in 1999 to 49 [kton] in 2020. For PM_{10} the emissions decreased from 17 [kton] to 16 [kton] and for the $PM_{2,5}$ the emissions decreased from 7 [kton] in 1990 to 4 [kton] in 2020. Focusing now to reduce $PM_{2,5}$ emissions by nearly zero has become an important matter because of the toxicity of these particles and their danger to humans and the environment.[15]

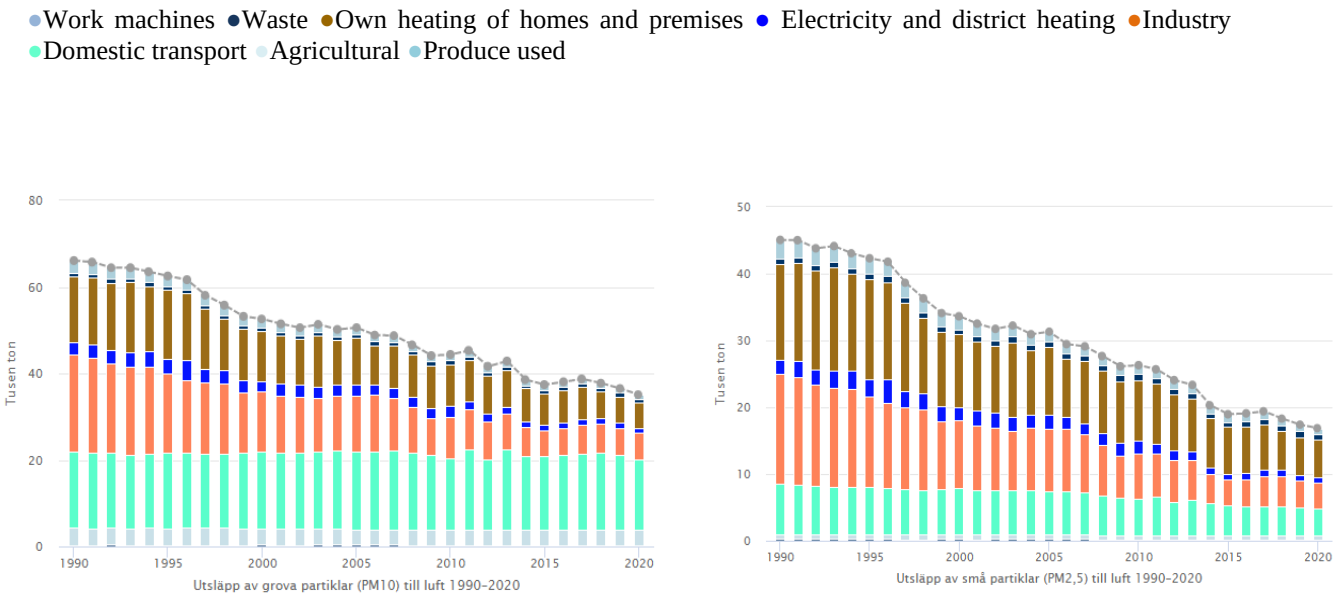

Figure 2: The left figure describes emission level for PM_{10}, the right figure describes emission level for $PM_{2.5}$ between 1990-2020

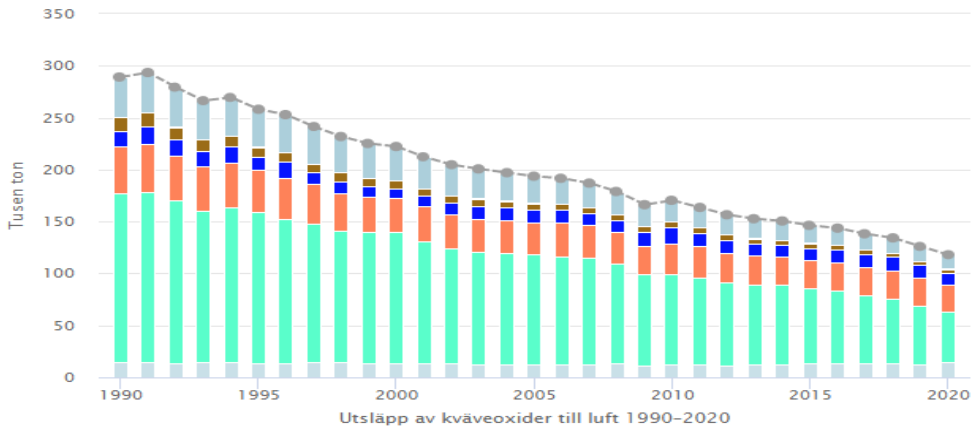

Figure 3: Emission level for NOx between 1990-2020

2.Theoretical Background

2.1 Exhaust Gas Recirculation (EGR)

The exhaust gas recirculation (EGR) technology is used in diesel engines of different sizes to control nitrogen oxide NOx emissions. The EGR system consists of control valves and a cooler, where emissions from the combustion process are re-mixed with the air entering the engine after reducing its temperature through the coolant.[16]

One of the most important reasons for reducing nitrogen oxide emissions is the decrease in the local maximum temperature because of the decrease in the amount of oxygen, as the process of mixing the exhaust gas with the air entering the combustion chamber leads to a decrease in the mass of oxygen and an increase in carbon dioxide[8]. Figure 4 below explains the effect of EGR on the flame area, where the difference in the spread of fuel appears more in the case of using the EGR with a lower amount of oxygen.

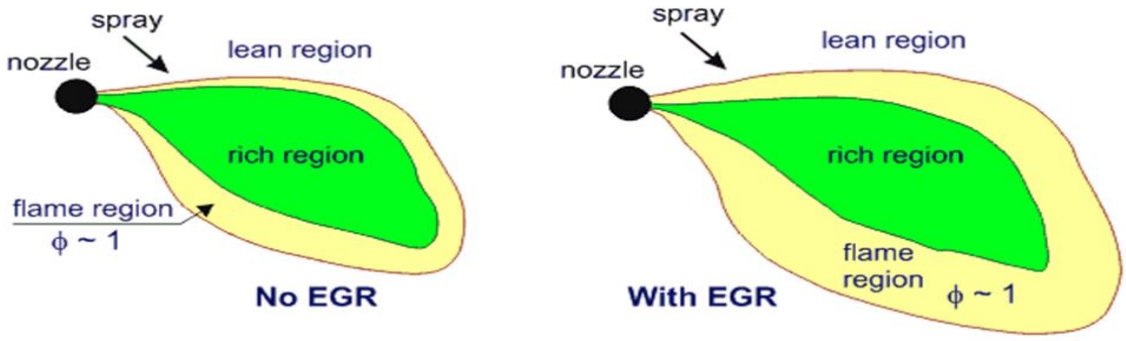

Figure 4: The effect for EGR on diesel flame[16]

The effect of EGR on reducing the percentage of nitrogen oxides is extensive and under all loads, and the higher the rate of EGR, the lower the percentage of nitrogen oxides, but this good effect on reducing the rate of nitrogen oxides harms PM emissions, where the percentage of emissions increases by about 45% [17]. Figure 5 below shows the effect of the EGR on nitrogen oxides and PM.

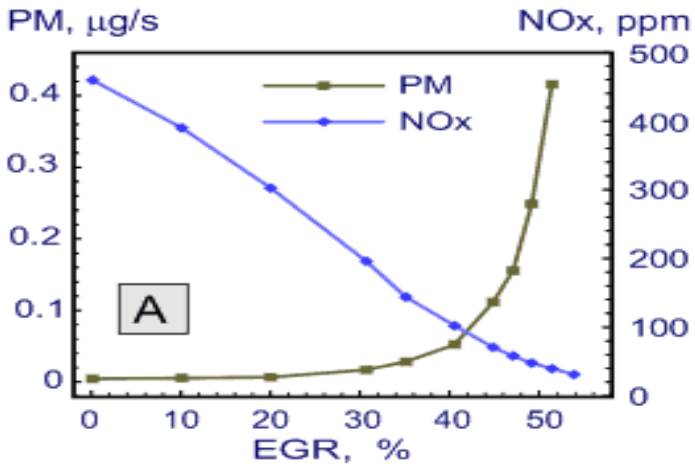

Figure 5: The effect of EGR on NOx and PM [10]

The exhaust gas recirculation (EGR) technology succeeds in reducing nitrogen oxides. However, it leads to other harmful emissions, as the gas released contains several harmful elements: HC, PM, CO the EGR technology is not considered sufficient, and another technology such as SCR must be used to reduce the risk of emissions, as mentioned in section 1.5.

2.2 Diesel Oxidation Catalyst (DOC)

Hydrocarbons (HC) and carbon monoxide (CO) are oxidized to carbon dioxide and water and converted into harmless products inside the DOC. The primary function of the diesel oxidation catalyst is its ability to oxidize the components of the exhaust gas coming from the EGR by using the oxygen which already exists in diesel exhaust. At low temperatures, there is no catalyst activity, and with the temperature of the exhaust gas rising, the process of oxidation of CO and HC begins as the temperature increases; the oxidation rate increases to eventually stabilize [18] , and this can be seen in Figure 6, which shows the development of the oxidation process for both HC and CO.

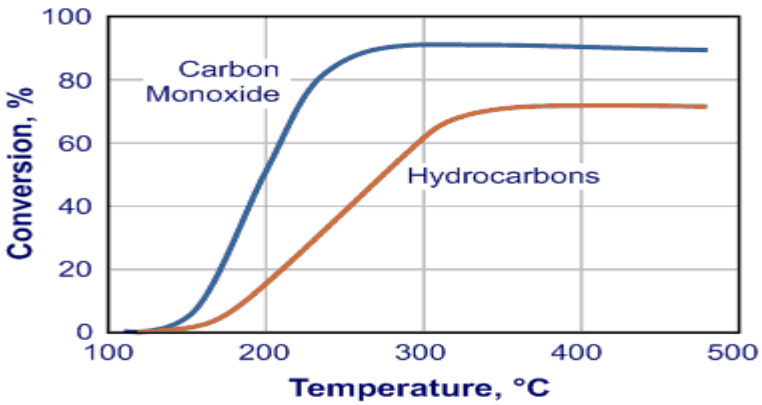

Figure 6: Temperature effect on the oxidize process for HC, CO [11]

The other primary function of the DOC is nitric oxide (NO) oxidation and its conversion to nitrogen dioxide NO_2. Unlike the HC and CO, the DOC dose does not reduce the NO_X until the following chemical reaction occurs: $2NO + O_2 \rightarrow 2NO_2$ .This leads to an increase in the proportion of NO_2, which in turn increases the proportion of the NO_2 /NO_X ratio coefficient [19] [18] , which is presented in figure 7. This increase of NO_2/NO_X led to better performance for the DPF to oxidation of the particulate matter and better performance for the SCR

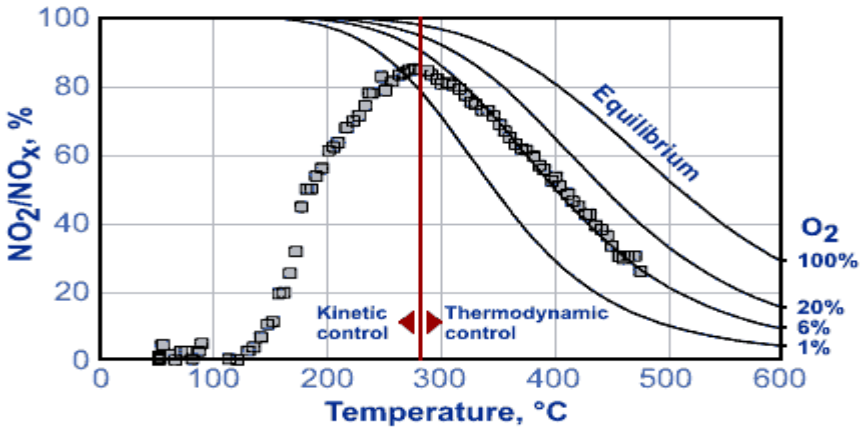

Figure 7: Show the oxidation of NO to NO_2 [12]

The DOC does not affect the particulate matter significantly, where the rate of soot oxidation is lower than other elements due to temperature. Therefore, it is challenging to obtain oxidation. To dispose of the toxic elements that remain in the exhaust gas after it leaves the DOC, the diesel particulate filter system is used, the procedure for which is described extensively in the following section [20]. The following figure explains in a simplified way the elements entering and the resulting elements after the outlet of the DOC.

Figure 8: The elements inlet and outlet of the DOC

2.3 Diesel Particulate filter (DPF)

The diesel particulate filters are used to capture diesel particulates and prevent them from spreading into the air. Currently, the diesel particulate filters have been developed to be effective in reducing toxic emissions, specific the PM from diesel engine's gas exhaust [18] . The main components of the particulate matter are the solid fraction (SOL); some consist of ash and carbonaceous material. The second element is the organic fraction (OF), which includes organic material obtained from fuel and oil [6]. The last fraction is sulfate particulate (SO_4) which includes water and the acid, as shown in figure 9 below

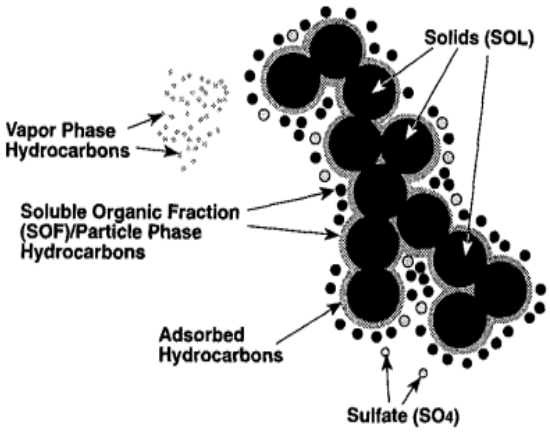

Figure 9: Schematic of particulate matter [21]

The diesel particulate filter consists of a ceramic wall-flow monolith placed in a compact form with each other. This design gives greater efficiency to the filter, and the flow is better controlled due to the design of the channels in an alternating manner where the beginning of the channel is open. However, the outlet is closed, thus forcing the gas to flow through the porous wall and capture the most significant number of particles [12, 18]. The following figure 10 shows how the gas passes through the wall using a method of wall-flow.

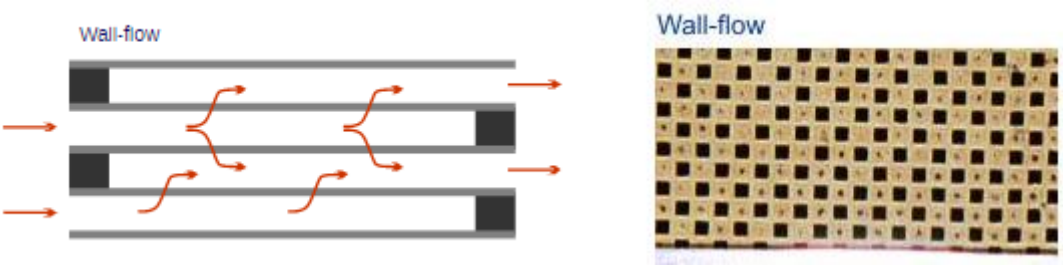

Figure 10: The gas flow by using the Wall-flow filter [11]

The capture of particles carried by the gas passing through the walls is done using two types of filtrations. The first is the filtration with a deep-bed filter, and in this filter, the particles with a diameter smaller than the diameter of the pores are captured in the filter and thus allowing the particles to precipitate and are helped by the way the small particles move in a non-uniform way and thus capture as many particles as possible. The other method is surface filtration or

cake filtration; this method begins after the loaded soot builds up the cake layer; this method is highly filtering efficiently. The pressure decreases steadily with the thickness of the dough increases [18]. Figure 11 shows how the particles are grouped in each method mentioned above.

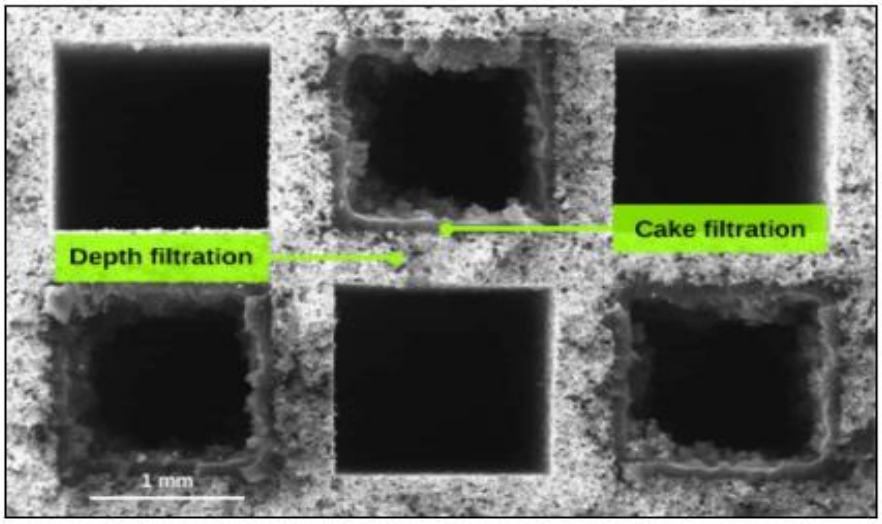

Figure 11: Loaded soot by Depth filtration/Cake filtration [11]

Using NO_2 as an oxidizer instead of oxygen will result in higher oxidation rates for soot and at a lower temperature than needed if oxygen is used. The oxidation temperature of the carbon in the soot is between 250-300 if NO_2 is used, while the required temperature is more than 550 if oxygen is used [22]. The diesel particulate filter effectively reduces the particulate matter where the reduced ratio reaches more than 90% [22]. Figure 12 presents the difference in the number of particles using the DPF and without the DPF.

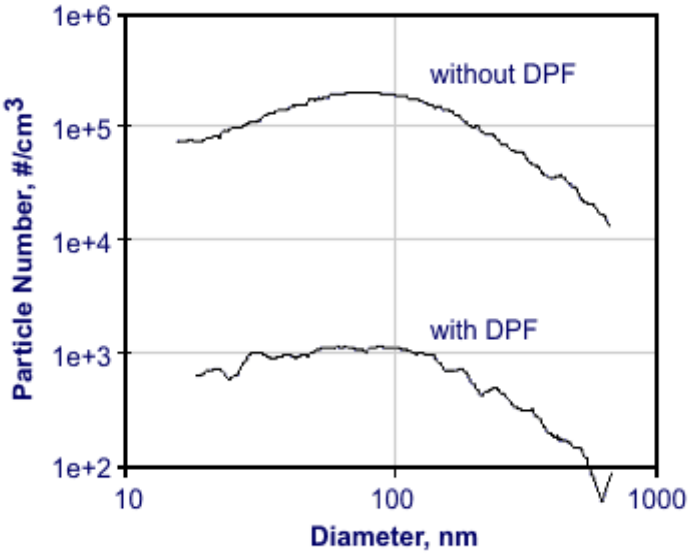

Figure 12: Different of Particles number with/without DPF [11]

2.4 Selective Catalytic Reduction (SCR) & Ammonia Slip Catalyst (ASC)

The selective catalytic reduction is one of the most successful techniques in removing many nitrogen oxides from gases through urea, which is decomposed into form ammonia NH3. The mixing process takes place when gas is passed inside the SCR, and this reaction results in the conversion of nitrogen oxides into nitrogen and water. The reactions inside the SCR depend mainly on temperature. Therefore, the efficiency of the SCR is affected by the temperature change, considering the temperature required for the reaction to occur between ammonia and nitrogen oxides. The reaction within the SCR needed a huge amount of urea to ensure that nitrogen oxides were eliminated as much as possible. However, there is an excess amount of ammonia that is not oxidized inside the SCR. Therefore, the ammonia slip catalyst (ASC) system is used to get rid of the unwanted amount of ammonia by oxidizing it and converting it to N_2 and H_2O [19]. The design for SCR-ASC system was described above in Figure 1 and the same figure also shows the elements entering at the beginning of the system and the elements leaving after.

3. Modeling Features

This section will explain the chemical reactions inside the DOC and DPF and the equations used to calculate the different parameters in the Axisuite program used during this project.

3.1 Catalyst Reactors

The catalyst is defined as a medium that helps complete the reaction. The catalyst is not a product of the reaction of the material involved but only an auxiliary medium to complete the chemical reaction. During the reaction, the reactants pass through activation energy, which is a heat barrier that helps form the final products of the reaction, considering that the catalyst does not affect the following factors.[23]:

ΔH The reaction enthalpy

ΔG Reaction free energy

K_e The equilibrium constant

In the diesel particulate filter, the catalysts used are heterogeneous catalysts composed of solid and heat-resistant materials, and reactions often occur on the surfaces of solid materials. There are two types of catalysts, homogeneous catalysts, and heterogeneous catalysts. The homogeneous are catalysts that have the potential to interact with reactants during the occurrence of the reaction and thus dissolve the catalyst. In contrast, to a heterogeneous catalyst, the reaction takes place in a different phase in the case of a heterogeneous catalyst. Therefore, the catalyst does not react with the reactants.[21]

In most catalysts, the surface layer of the catalyst is coated with catalytic materials such as aluminum oxide AL_2O_3 and Platinum Pt as shown in the figure below.

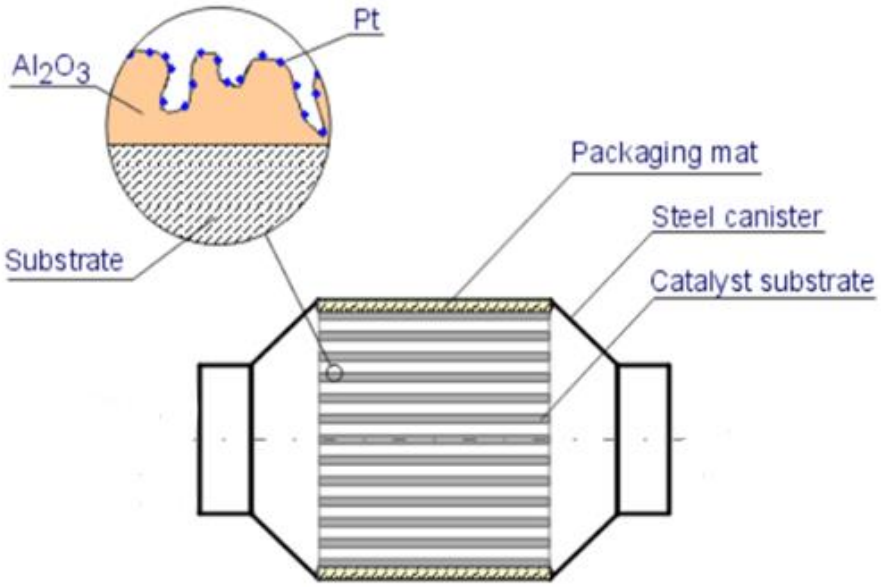

Figure 13: Graphic of catalyst transformer [20]

3.2 Diesel oxidation catalyst (DOC)

The diesel oxidation filter used during the experiment is the DOC for the D13 Volvo engine HD Diesel type, as shown in Figure 14, considering the channel width, height, and channel wall thickness.

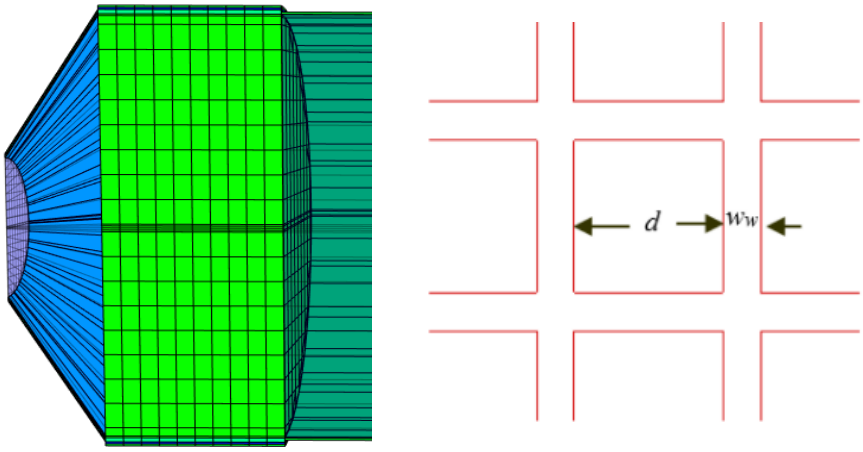

Figure 14: Diesel oxidation catalyst geometric

3.2.1 Reactions

As present in the theoretical section, the main task of the DOC is to oxidize both carbon monoxide and gas-phase hydrocarbons and the organic fraction by using oxygen. The following main reactions explain how this process occurs within the catalyst.

$$NO + 0.5\,O_2 \rightarrow NO_2 \qquad (1)$$

$$C_3H_6 + \left(\frac{9}{2}\right) O_2 \rightarrow 3CO_2 + 3H_2O \qquad (2)$$

$$CO + 0.5O_2 \rightarrow CO_2 \qquad (3)$$

The rate reaction in general can be thought using the following equation:

$$R = \frac{k.\mathrm{P_A}.P_B}{T.G} \quad (4)$$

Where the K is Arrhenius term $K = A.e^{-\frac{E}{\Re T}}$ and $P_A = \frac{P_A}{P_0}$ the ratio pf partial pressure and G is inhibition expression. For the reactions above the rate reactions for HC, CO, NO is present as following:

$$R_{No} = \frac{k_{NO}.P_{NO}.P_{O_2}^{0.5} - K_{NO}.P_{NO2}}{G} \quad (5)$$

$$R_{CO} = \frac{k_{CO}.P_{CO}.P_{O_2}^{0.5}}{G} \quad (6)$$

$$R_{HC} = \frac{k_{HC}.P_{HC}.P_{O_2}^{0.5}}{G} \quad (7)$$

See Axisuite manual section rate expression Table 1.

3.2.2 Flow

To calculate the flow in the DOC, the *Axisuite* software uses an advanced flow calculation algorithm. The exact time of the inflow is predicted concerning the flow velocity inside the catalyst is calculated by calculating the flow resistance within the stacked catalyst layers. The heat field inside the catalyst plays an essential role in calculating the flow using the resistance calculation method.

3.3 Diesel Particulate Filter (DPF)

The design method of the DPF ensures the highest effectiveness in capturing PM where the channel inlet is open, and the output is blocked, forcing the particles to pass through porous walls painted with a catalyst material. This way helps to capture a large number of particles. The ceramic monolith type of diesel filter is the most used to remove the particulate matter from the diesel exhaust. Figure 15 presents the design for DPF and simplifies how it works.

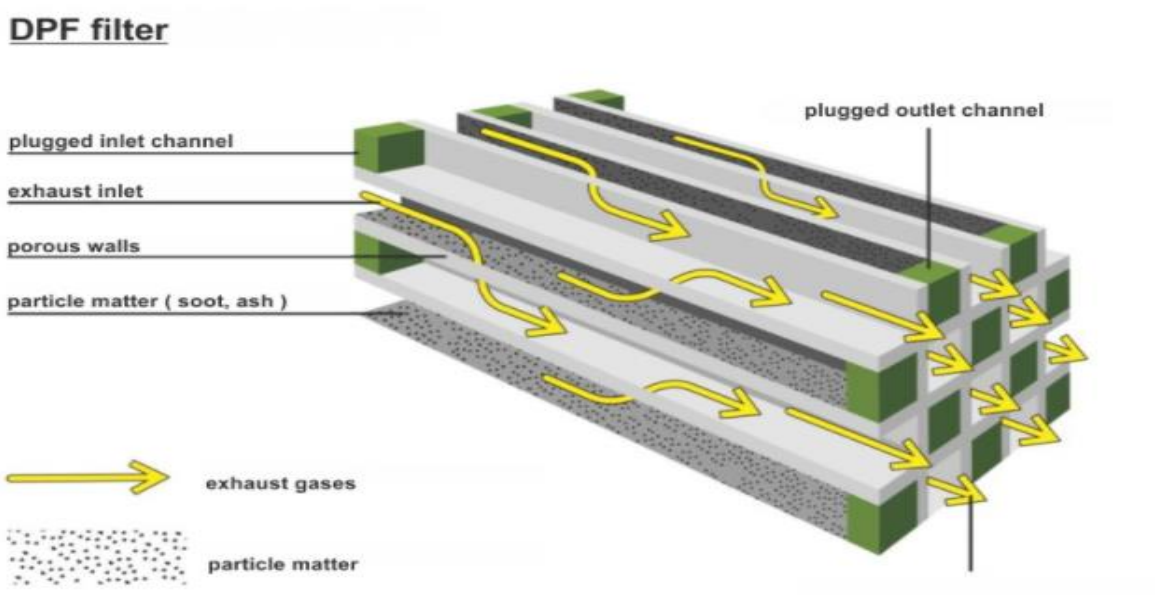

Figure 15: Diesel Particulate Filter [24]

3.3.1 Reactions

As described in the theoretical part of the diesel particulate filter, the DPF oxidized the soot, and this happens through the oxidation of oxygen O_2 and NO_2. The following reactions present how the DPF oxidized the soot by using the oxygen:

$$C + O_2 \rightarrow CO_2 \quad (8)$$

$$C + \frac{1}{2}O_2 \rightarrow CO \quad (9)$$

The previous equations describe the so-called active renewal. Oxidation using oxygen requires high temperatures of about 600 degrees Celsius to react in a short time, and soot oxidizes completely, while at low temperatures, the reaction rates are slow, and soot does not completely oxidize [19]. The effect of temperature can be explained by the equations of the rate of reactions as presented below:

$$r = K.[C]^a.[O_2]^b.[H2O]^c \quad (10)$$

Where: $[H_2O\ ]$ & $[O_2]$ focus mol/mol, [C] quantities of soot /mol, [K] reaction rate constant [a, b, c] order of reactions.

The soot oxidizes fast with NO_2 and with a low-temperature degree of regeneration (250 degrees Celsius) compared to oxygen. The following equations present the reactions by using nitrogen dioxide:

$$NO + \frac{1}{2}O_2 \rightarrow NO_2 \quad (11)$$

$$NO_2 + C \rightarrow NO + CO \quad (12)$$

$$CO + \frac{1}{2}O_2 \rightarrow CO_2 \quad (13)$$

3.3.2 Flow

To calculate the flow in the DPF, the *Axisuite* software uses an advanced flow calculation algorithm. The exact time of the inflow is predicted concerning the flow velocity inside the catalyst is calculated by calculating the flow resistance within the stacked catalyst layers. The heat field inside the catalyst plays an essential role in calculating the flow using the resistance calculation method. Concerning the pressure drop, the program uses the same algorithm to calculate the pressure drop, energy, and mass, which will be explained in more detail below.

3.3.3 Mass and momentum balance

To predict the pressure, drop, mass, and momentum is calculated. A study is divided into the first stage, when the gas enters the pores of the catalyst, and the second, when the gas exits from the walls of the catalyst, as shown in Figure 16.

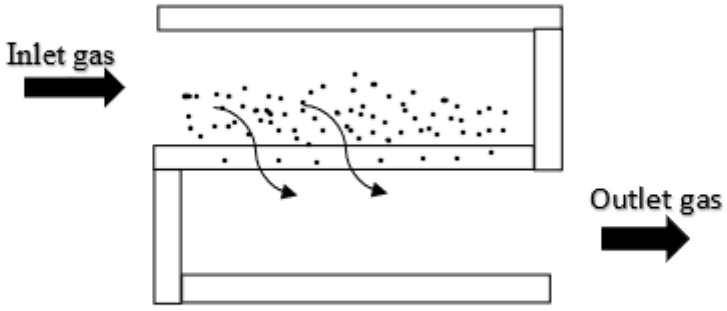

Figure 16: Gas flow through DPF wall

The equation of mass balance for the gas flowing into the inlet and outlet channels is defined as shown in Figure 6 as follows:

$$\frac{\delta}{\delta Z}(\rho_i v_i) = (-1)^i . \frac{N}{d} (\rho_w v_w) \qquad (14)$$

The equation of monument balance for the gas flow into the inlet and the outlet is present as:

$$\frac{\delta p_i}{\delta_Z} + \frac{\delta}{\delta_z(\rho_i v_i^2)} = -\frac{\alpha_1 \mu v_i}{d^2} \qquad (15)$$

See Axisuite manual equations NO 364 and 365.

Table 2: Describes symbols of the mass and momentum calculations

ρ	$Density\ [kg/m^3]$
v	$Gas\ velocity\ [\frac{m^2}{s}]$
N	$Number\ of\ permeable\ sides$
ρ_w	$Density\ of\ deposit\ inside\ the\ wall\ [\frac{kg}{m^3}]$
v_w	$velocity\ of\ deposit\ inside\ the\ wall\ [\frac{m^2}{s}]$
α	$thermal\ diffusivity\ [\frac{m^2}{s}]$
d	$Hydraulic\ diamter\ of\ a\ clean\ channel\ [m]$
μ	$Dynamic\ viscosity\ [Pa.s]$

3.3.4 Pressure Drop

The pressure drop is one of the most critical factors in soot oxidation within the DPF. The pressure drop starts to increase when the soot begins to form, where the total pressure drop consists of several pressure drops in different stages. According to Figure 17, all different pressure drop is presented.

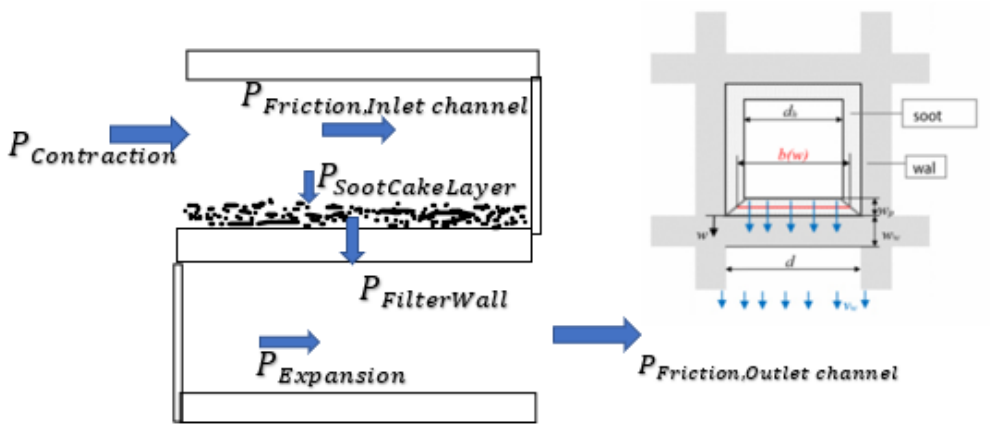

Figure 17: Total pressure drop inside the DPF

The following equations present the different pressure drop phases inside the diesel particulate filter [25]. Table 2 present calculation forum for all pressure drop. See Axisuite manual section equations NO 156 to 165.

Pressure Drop	Calculations forum
$P_{Friction\ in\ inlet\ channel}$	$\frac{\mu Q}{2V_{trap}}(d_h + w_{wall})^2 \frac{4Hl^2}{3}(\frac{1}{(d_h - 2w_{soot})^4})$
$P_{Friction\ in\ outlet\ channel}$	$\frac{\mu Q}{2V_{trap}}(d_h + w_{wall})^2 \frac{4Hl^2}{3}(\frac{1}{(d_h)^4})$
$P_{soot\ cake\ layer}$	$\frac{\Re T}{M_g \rho^-}\left(\frac{\mu d \rho_w v_w}{2K_p P^-}\right)\ln(\frac{d}{d_h - 2w_p})$
$P_{FilterWall}$	$\frac{\mu Q}{2V_{trap}}(d_h + w_{wall})^2.(w_{wall}/K_{wall}.d)$
$P_{contraction}$	$\frac{(\xi_c \cdot \rho_{inlet} v_{inlet}^2)}{2}$
$P_{Expansion}$	$\frac{(\xi_c \cdot \rho_{outlet} v_{outlet}^2)}{2}$

In the equations defined above, the permeability of particulate K_p and the permeability of the wall K_w. The permeability of particulate K_p depends on the temperature and pressure of soot as present in the equation:

$$K_p = K_{p,0}\,(1 + \frac{C_4\,P_0}{P}\mu\sqrt{\frac{T}{M_g}}) \qquad (16)$$

The permeability of the wall K_w depends on pressure and temperature, but considering the addition of the correction factor for the sudden drop in wall permeability as shown in the following equation:

$$K_w = \frac{1}{(\frac{1}{K_{w,0}} + C_1.\rho_p + C_2.\rho_p^2)}(1 + C_4.\frac{P_0}{P}\mu\sqrt{\frac{T}{M_g}}) \qquad (17)$$

The particulate layer thickness w_p defend as the following expression:

$$W_p = \frac{1}{2}\left(d - \sqrt{d^2 - \left(\frac{2m_p}{\rho_p V_{trap} CP_{sm}}\right)}\right) \qquad (18)$$

Table 3: Describes symbols of the pressure equations

c_4	$Slip\ correction\ factor\ [\frac{ms}{(\text{kg moleT})^{0,5}}]$
V_{trap}	$Effective\ trap\ Volume\ [m^3]$
w_w	$Substrate\ wall\ thickness\ [m]$
w_p	$Soot\ Layer\ thickness\ [m]$
T	$Temperature\ [K]$
$\Re$	$Gas\ constant\ [\frac{J}{molK}]$
ξ	$Additive\ concentration\ in\ deposit\ Layer$
d_h	$Hydraukic\ diameter\ of\ a\ channel[m]$
H	$Heat\ source\ component\ [\frac{w}{m^3}]$
l	$Channel\ length\ [m]$

3.3.5 Energy Balance

There are two expansions for the energy balance under the solid phase, and both equations are related to the thermal conductivity equation for the filter. The first equation is formulated in the case of polar coordinates and used with 2D simulations.

$$\rho_s . C_\rho, s \, . \frac{\partial T_s}{\partial t} = \lambda_s, z \, . \frac{\partial^2 T_s}{\partial z^2} + \lambda_s . r . \frac{1}{r} . \frac{\delta}{\delta r} \left(r . \frac{\delta T_s}{\delta r} \right) + S \qquad (19)$$

The second energy balance construct with Cartesian coordinates and used with 3D simulations.

$$\rho_s . C_\rho, s \, . \frac{\partial T_s}{\partial t} = \lambda_s, x \, . \frac{\partial^2 T_s}{\partial x^2} + \lambda_s . y \frac{\partial^2 T_s}{\partial x y^2} + \lambda_s, z \, . \frac{\partial^2 T_s}{\partial z^2} + S \qquad (20)$$

For the energy balance for gas, the heat exchange with the channel walls is taken into consideration, and the amount of heat flowing into and out of the channel is calculated according to the following two equations. Equation 21 presents the gas volume through the inlet.

$C_p, g \, [d^2 \rho_1 v_1 T_1|_{z+\Delta z} - d^2 \rho_1 v_1 T_1|_z \, + 4d . \Delta z \rho_w v_w T_1|_z \,] = h_1 4d . \Delta z . (T_s - T_1) + H_{react}$

…. (21).

$T_1 = T_{inlet}$

For the gas volume in the outlet channel according to equation 22:

$T_2 = T_{out}$

$C_p, g \, [d^2 \rho_2 v_2 T_2|_{z+\Delta z} - d^2 \rho_2 v_2 T_2|_z \, + 4d . \Delta z \rho_w v_w T_2|_z \,] = h_2 4d . \Delta z . (T_s - T_2) + H_{react}$

….. (22) .

See Axisuite manual section energy balance equations NO: 382,383,409,411.

Table 4: Explain symbols for energy balance equations

C_p	$Specific\ heat\ capacity\ [\frac{J}{KgK}]$
λ	$Thermal\ conductivity\ [\frac{W}{mK}]$
S	$Heat\ soure\ term\ [\frac{W}{m^3}]$
v	$exhaust\ gas\ velocity\ [\frac{m}{s}]$
H_{react}	$Reaction\ heat\ \left[\frac{J}{mol}\right]$
d	$Hydraukic\ diameter\ of\ a\ channel[m]$

3.3.6 Soot Mass Balance

Soot mass equilibrium includes soot consumption and soot accumulation, where soot molecules follow flow lines within the filter. The equation of the mass of soot some be used is illustrated in the following equation:

$$\frac{dm^p}{dt} = -m^p \sum R'_k + S_F \rho_{p,w} v_w \mu_p E \qquad (23)$$

$\sum R'_k$ Total of all soot oxidation reaction rates.

E Filtration Efficiency.

μ_p Concentration of soot particles.

See Axisuite manual section soot mass balance and properties equation NO 520.

4. Method

The literature study was carried out in the previous section, explaining how the DPF and DOC work and showing the chemical reactions inside the catalyst and the physical properties from pressure difference equations to mass and energy balance. For the simulations, Axisuite software was used, a commercial platform developed by *Exothermia* company based in Thessaloniki.

The *Axisuite* platform runs the exhaust after-treatment system simulations in its various parts (DOC, DPF, SCR). In the first stage, the simulation model was wholly built to match the actual shape used in the laboratory concerning the shape's dimensions and adjusting other parameters to be compatible with what is used in the experiment, as presented in Table 5.

Table 5: Specifications of DOC and DPF

Parameter	DOC	DPF
Catalyst type	Pt	Pt
Cell density	400_4_Square	400_4_Square
Diameter (Inch)	12	12
Length (Inch)	4.5	12
PGM g/ft3	3	10

Where PGM: Platinum group metal. Pt used to guarantee high nitrogen dioxide formation rates and low regeneration temperatures.

The next step is to use the measured data from the experiments for the simulations of the model built using the software Axisuite. Input parameters measured in experiments consist of input temperatures, mass flow rate, and concentration of NO, NO2, O2 and Soot emissions. In line with the input parameters to get the simulation results and compare them with the experimental data to find out the percentage of match between them and try to influence the different input parameters to get better results.

Figure 18 shows combining the DOC and DPF regarding the critical information considered. The DOC input data, including mass and temperature concentrations, were taken from the data measured in the experiment. The pressure difference was measured before and after the DPF. There are no additions for the pipe between the DOC and DPF, so no modifications will be made to the parameters leaving the DOC and entering the DPF.

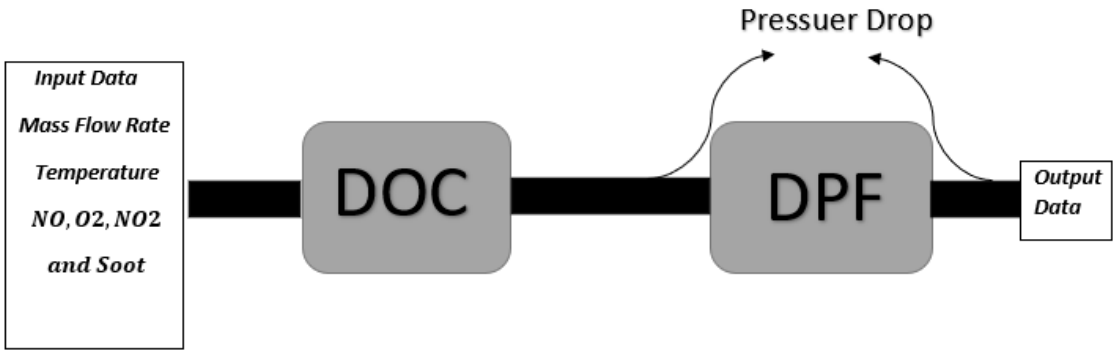

Figure 18: Describe the model and measure data

4.1.1 Test Cycle

Different test cycles are being used to produce cell data for emission certification. These cycles vary according to the engine type (Heavy-Duty Engines, Heavy-Light Engines). In the case of heavy diesel engines, there are several test cycles used in the EU, like the Nonroad transient cycle (NRTC) and European stationary cycle (ESC). The NRTC is a test cycle used to certify emissions of diesel engines whereby torque and engine speed are measured at different points within a specified time.[26]

The European stationery is a test cycle for measuring emissions from heavy diesel engines. Data is collected by switching engine speeds and torque in 13 different positions (A100, B50, B75, A75, Etc.). Emissions from each position are measured and averaged based on the number of emissions produced by the engine.[27]

In this project, the Volvo D13 engine was used to collect test cell data and validate the model that was previously developed using the Axisuite software. Professor Jonas Sjöblom developed the test cycle method to collect the data. This is a custom-made test cycle where data is collected at multiple locations. The speed and load are different, different locations are swapped around selected points and data is collected within a specified time, as illustrated in Table 6. The selection test cycle is used for research and is not an approved emissions certification course.

Table 6: Test cycle modes.

Mode	Engine speed [rpm]	Load [Nm]	Time [m]
A25	1200	662	12
A100	1200	2560	12
A25	1200	662	12
C25	1800	528	12
C75	1800	1582	12
Change to Euro I			
A25	1200	662	12
Change to Euro VI			
A100	1200	2560	12
A25	1200	662	12

4.1.2 Material and insulation

The DOC and DPF are designed to match the components used in the experiment and the type of tests to reach the best results. The temperature range for the inside the DOC, DPF, was assumed to be between 300 [k] & 700 [k] and to fit these assumptions, the Cordierite P35 was used for the DOC and Sic NGK P52 d20 for the DPF. The insulation and the canning over the substrate and both DOC and DPF are characterized in Figure 19a. The first layer is a cover layer for both the DOC and DPF built by using Steel which withstands high temperatures and thickness of 1.5 mm. The second layer was insulation, where insulating materials were added to the DOC and DPF, and in both cases, the materials were Fiber Mat. The canning layer from Steel (AISI316) with a thickness equal to 1.5mm was added to both the inlet and outlet cone. Figure 19b presents the DOC-DPF model that was used during the experiment and A cross-section showing the design of the DOC-DPF model in Axisuite.

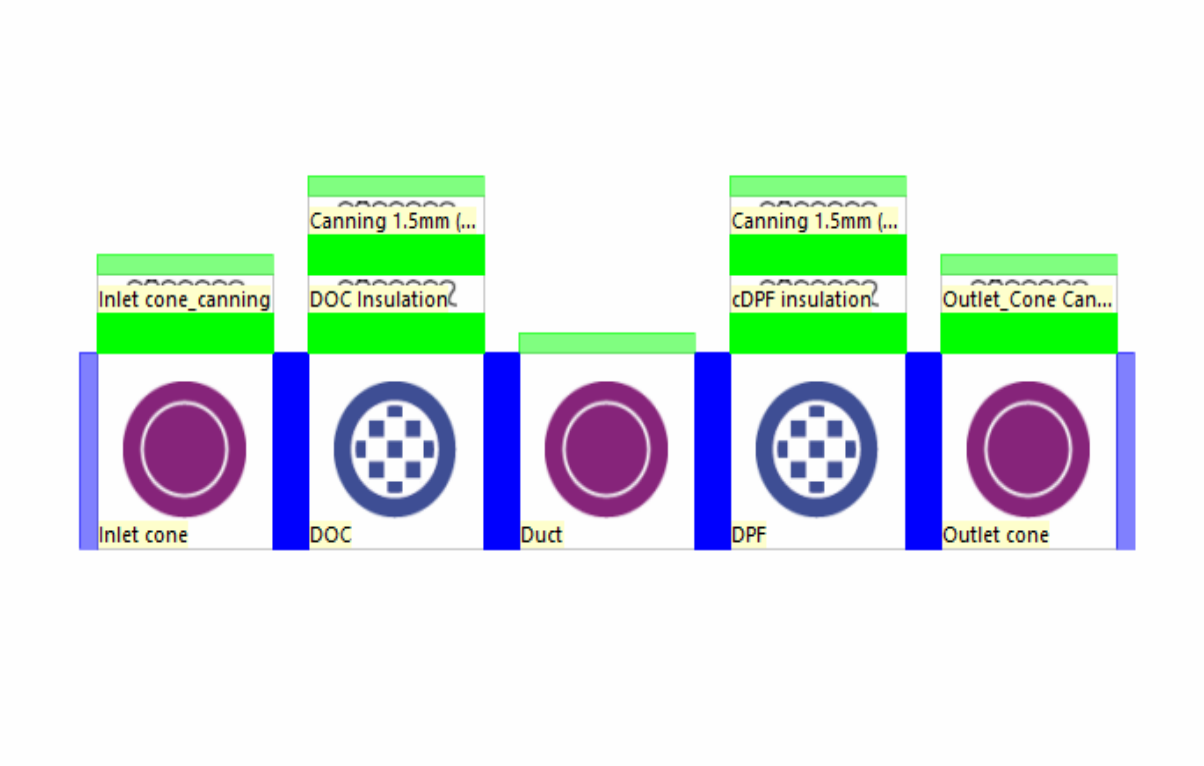

Figure 19a: Present Canning & Insulation used in the model.

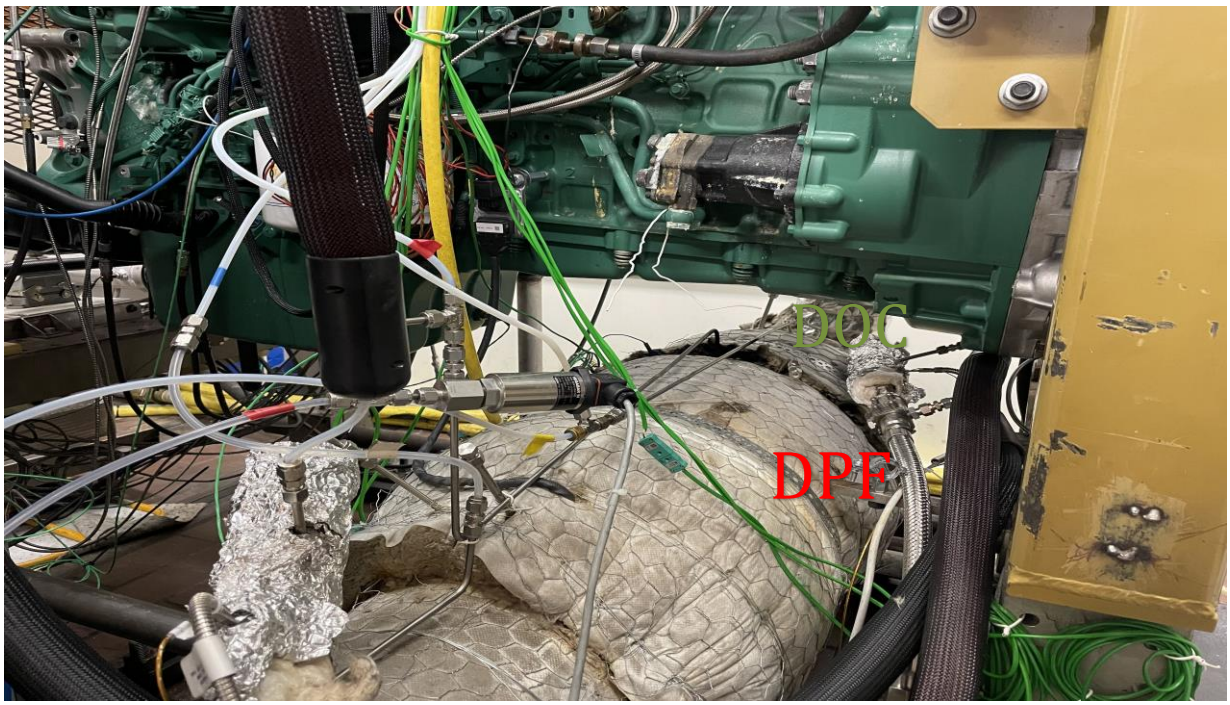

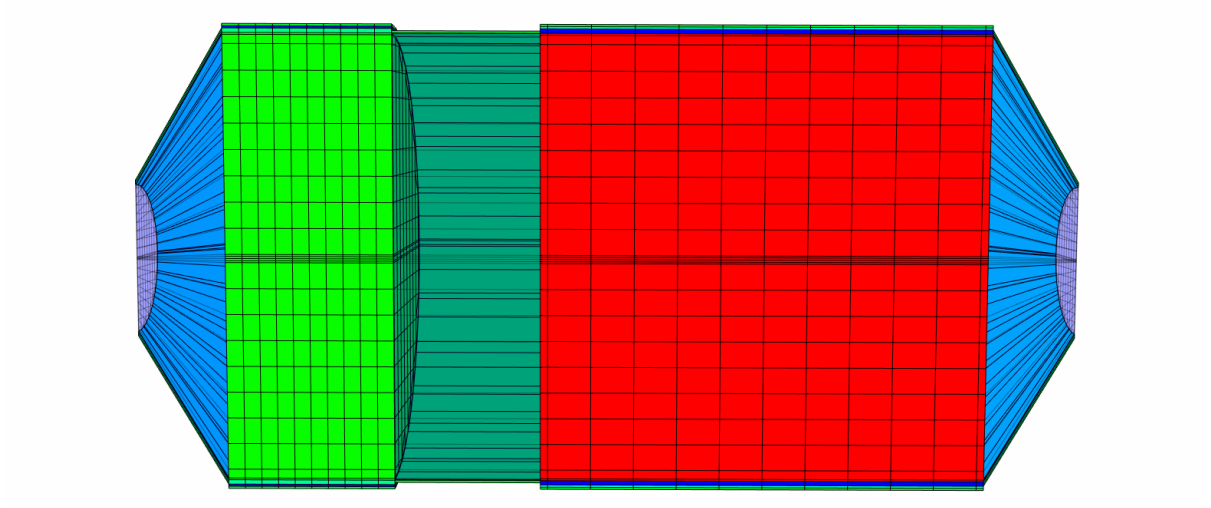

Figure 19b: The A cross section showing the design of the DOC-DPF model in *Axisuite*. The real DOC-DPF system which was used during the experiment.

4.2 DOC & DPF Model

In this section, design specifications will be displayed for both the DOC, DPF and the different input conditions. In addition to the local boundary and the applied methods to improve different parameters.

4.2.1 Model Specifications

The model was designed using *Axisuite* according to Figure 21, where the model consists of the input data, DOC, DPF filter, and output data. The input data includes time, mass flow rate, temperature and soot concentrations. The next component (DOC-DPF) is the filter designed individually according to specifications data in Table 5. The DOC was connected to an inlet cone and the outlet cone was placed after the DPF. To connect the catalyst parts, the duct was placed between the DOC and the DPF as illustrated in Figure 20.

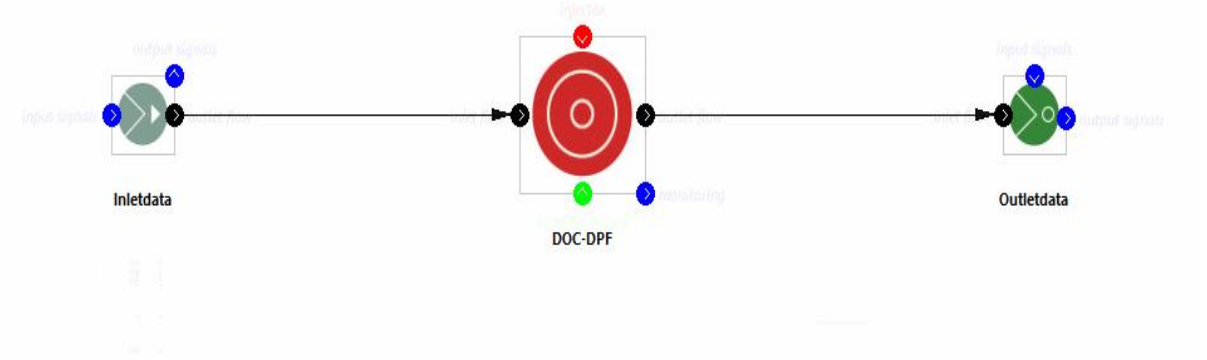

Figure 20: Model of DOC & DPF in AxiSuite. The flow comes into the Inlet Con to the DOC - DPF. The flow leva out at the outlet cone as presented in Figure 20.

All chemical reactions mentioned above were set within the model to obtain whole reactions necessary for the filters to oxidate the soot. The porous medium model was selected as Sphere, and the diffusion model activated and selected as mixed diffusion. The internal model of wall permeability was used, which uses a polynomial-type function to calculate the wall permeability, allowing the adjustment of the wall's permeability to suit the mass flow rate. Furthermore, the soot properties have been tuned to meet the Euro VI emission, class.

4.2.2 Concentration of O2

The reaction form for diesel fuel present as:

$$CH_x + y\ O2\ \rightarrow CO2\ + H2O \quad (24)$$

To get the chemical equilibrium of the previous equation, each must be calculated by using the fuel characteristics used in the experiment and listed in the **Preem** quality certification according to Figure 42 in the appendix, where the amount of substance of carbon and hydrogen content is given and through using the quantity and mass calculation according to the following equation.

$$n_c = m/M_m\ = 86.2/12.011\ [m/m] \quad (25)$$

$$n_H = m/M_m = 14.54/1.008\ \ [m/m] \quad (26)$$

$$n_H/n_c =\ 2.004 \approx 2 = x\ \ [m/m] \quad (27)$$

To find out the volume of the remaining oxygen concentration, it is necessary to calculate the amount of concentration used and subtract it from the amount of oxygen entering, using the following equations. MATLAB was used to calculate the oxygen concentrations to be used as an input into the *Axisuite* model.

$$n_{fuel} = m/M_{fuel} \quad (28)$$

$$CH_2 + \frac{3}{2}O_2 \rightarrow CO_2 + H_2O \quad (29)$$

$$O2_{used} = 1.5 * m_{fuel}/M_{fuel} \quad (30)$$

The air fuel ration was calculated according to:

$$A/F = m_{air}/M_{fuel} \quad (31)$$

$$M_{air} = 21\% \,.O2 + 79\% \,N2 = 29\ [g/mol] \quad (32)$$

Now the concentration of O2 can be calculated through the following equation:

$$Y_{O2} = n_{O2,out}\ /n_{air} + 0.5n_{O2,used} \quad (33)$$

4.2.3 Concentration of NO&NO2

The NO_X data was measured during the experiment by using the NO_X sensor. When knowing the data on nitrogen oxides, it becomes possible to calculate the concentration of NO and NO_2, the NO_X molar fraction was primarily calculated by using the following equation:

$$NO_x = \frac{\frac{\dot{m_{NOx}}\left[\frac{g}{s}\right]}{MW_{NOx}\left[\frac{g}{mol}\right]}}{\frac{\dot{m_{exhaust}}\left[\frac{g}{s}\right]}{MW_{exhaust}\left[\frac{g}{mol}\right]}}$$

Where:

$\dot{m_{NOx}}\left[\frac{g}{s}\right]$ The NOx mass flow rate.

$MW_{NOx}\left[\frac{mol_{NOx}}{g}\right]$ The molecular weight of the NOx.

$\dot{m_{exhaust}}\left[\frac{g}{s}\right]$ The exhaust gas mass flow rate.

$MW_{exhaust}[\frac{mol_{exhaust}}{g}]$ The exhaust gas molecular weight.

In the case of heavy diesel engine as presented in this model the assumption of NO2 will be 10% from NOx out and the NO about 90 % [28] as the following:

$$NO_2 = 0.1 * NO_x$$

$$NO = NO_x - NO_2$$

4.2.4 Boundary Condition

The boundary condition for the model is the mass flow rate, measuring the inlet temperature and the Concentration of O2, NO2, NO and Soot before the DOC. The initial temperature for the mode was set to $400\,k$. The initial wall soot loading range was selected between $0 - 2.5 g/l$. The wall permeability was set as 8e-14 for the DOC, and a 3D mesh was used for both the DOC and the DPF. Figure 22a presents the initial mass flow rate that's used as input, and Figure 22b presents the initial temperature data.

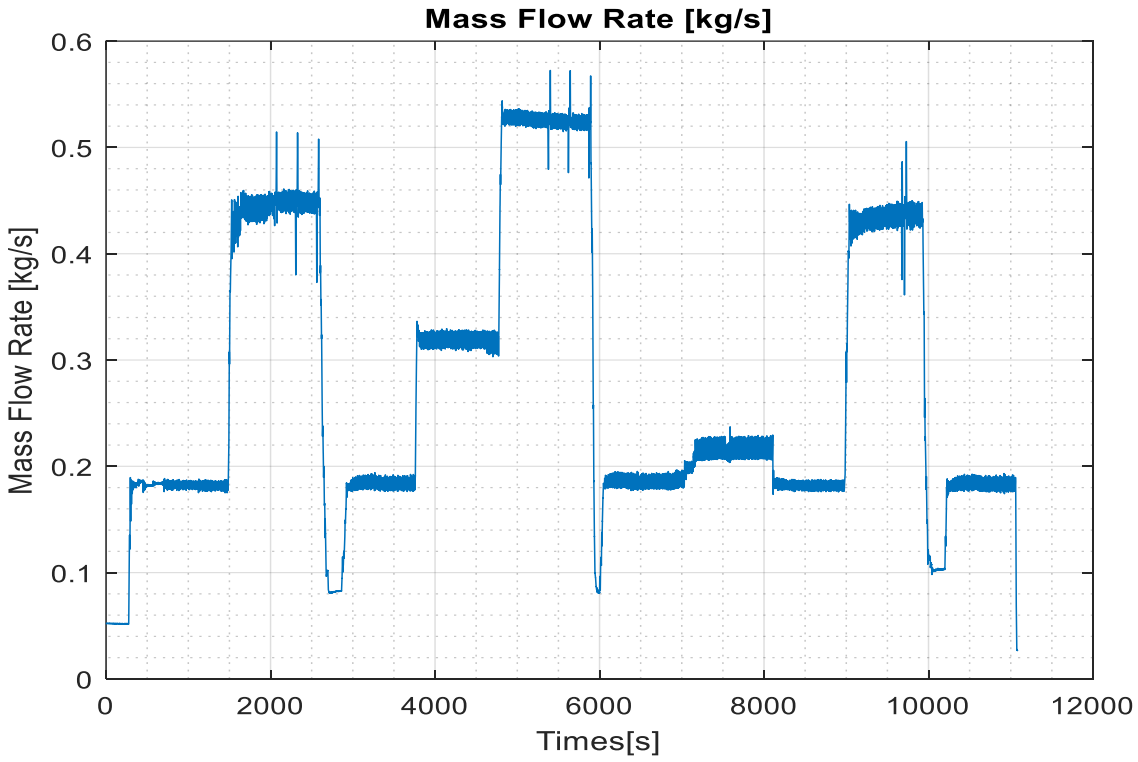

Figure22a: Mass flow rate [kg/s]

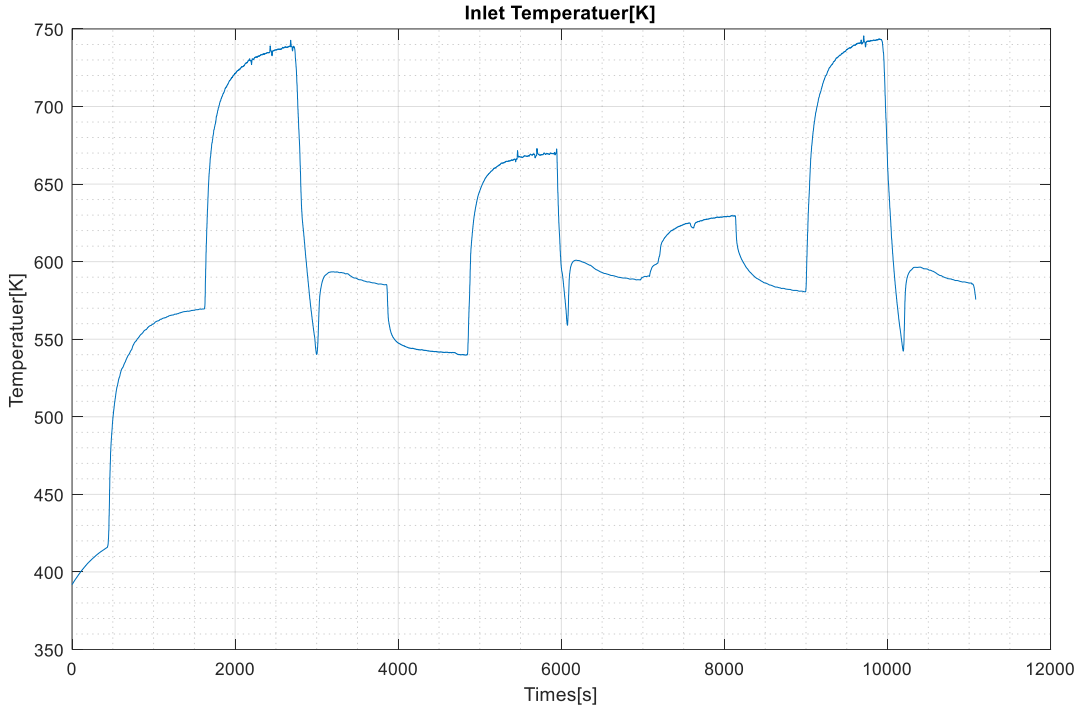

Figure22b: Inlet temperature [k]

4.2.5AVL Micro Soot

The MSS Plus system was used to measure soot concentration during the experiment, which is a photoacoustic technology operating on the photoacoustic principle that helps to measure soot concentrations as low as 1 $\left[\frac{\mu g}{m^3}\right]$ with high sensitivity and measuring range $[1 - 1000 mg/m^3]$[29]. Figure 23a illustrates the measure photoacoustic system. The measurement sensors were installed during the experiment: before the DOC, between the DOC-DPF, and after the DPF, where the device exposes gas samples to modified light to detect soot particles. Figure 23b illustrates the difference between the soot filter with capture and clean soot filters. [29]

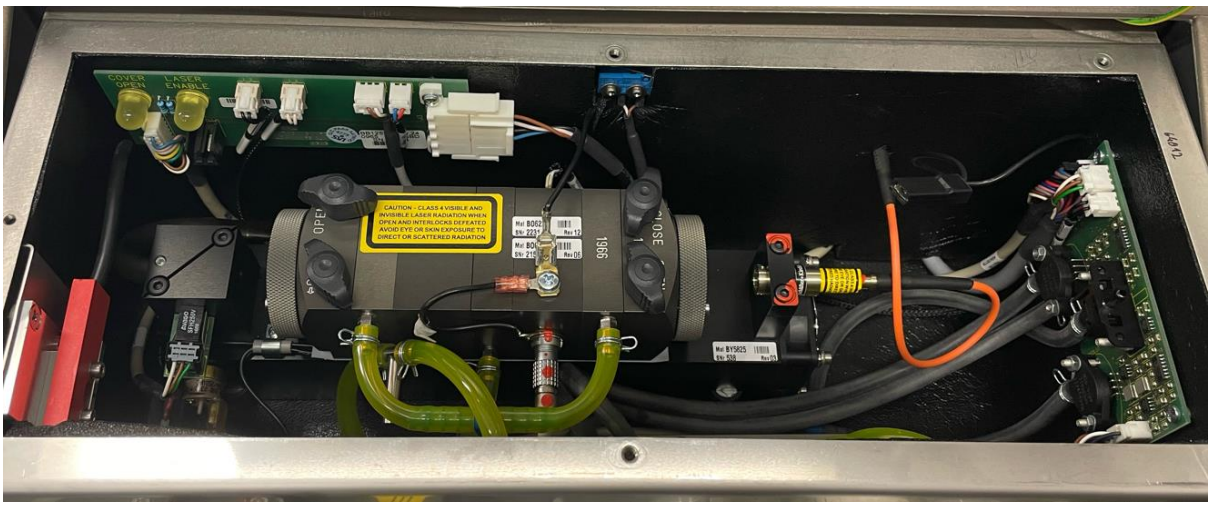

Figure 23a: The measure photoacoustic system.

Figure 23b: The filter with capture soot to the left photo vs the cleanly filter the right photo.

The data of soot concentrations collected by the AVL micro soot is shown in Figure 24. The data collected before the DOC was purified using MATLAB to reduce the percentage of fluctuations to ensure better results. After purification, the soot data was used as input data for the model in Axisuite. Figure 23 presents the soot data before filtering the blue line and the soot data after filtering the red line.

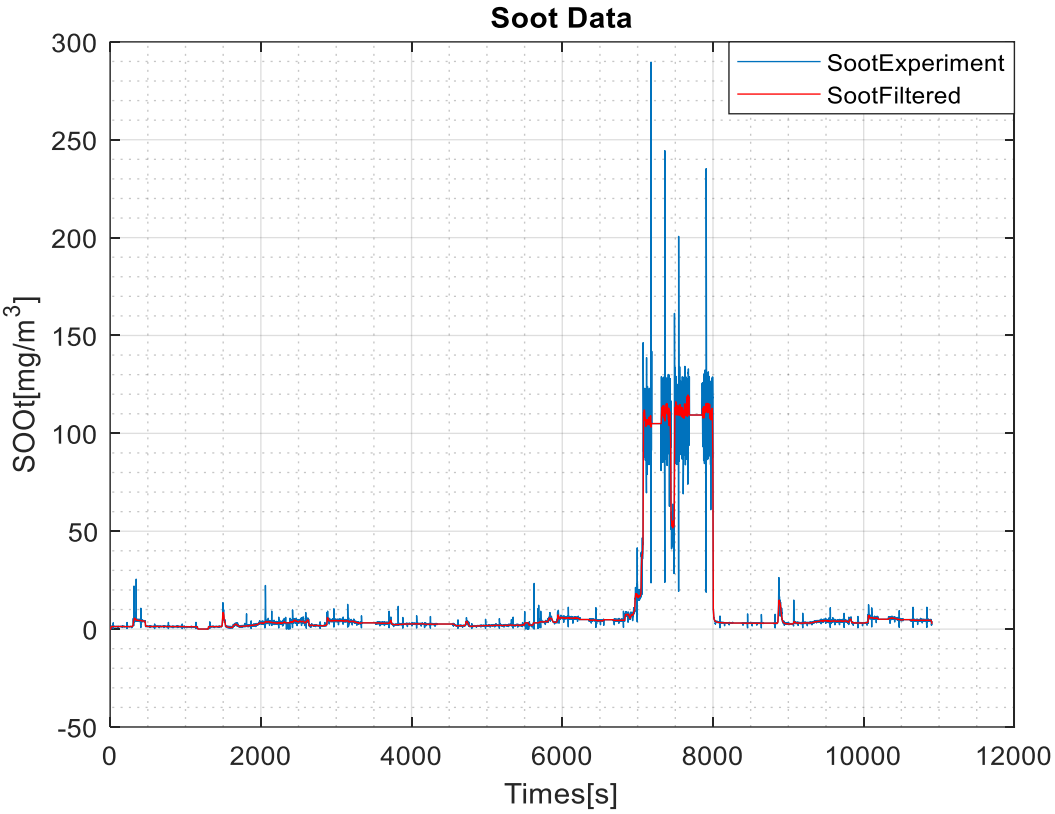

Figure 24: The soot data before filtered the blue line and the soot data after filtered the red line.

4.2.6 Parameter estimation

Within the framework of achieving the project's desired goals, many parameters can be modified that have a positive impact on the pressure drop and soot loading. Calculating the expected pressure drop requires solving the mass and momentum equilibrium equations mentioned in Section 3.3.3. The simulation was performed using the measurements collected during the experiments to predict the measured pressure drop for different temperatures and mass flow rates. The results showed that modifying the permeability of the wall $K_{w,0}$ as shown in Equation No. 17, affected the pressure drop as the modification of the wall's permeability leads to better control of the mass flow rate.

Since the deep filtration model was used for the model, which uses an engineering approach to calculating the filtration efficiency of the wall and soot cake, better filtration efficiency leads to better soot loading. The diffusion mechanism correction factor η_D and the interception mechanism correction factor η_R are two of the most critical factors that help to increase the efficiency of the filter. According to the following equation, higher values of the diffusion mechanism correction factor increase the filtration efficiency of small particles:

$$\eta_D = \eta_{clean,D} 3.5 \left(\frac{\varepsilon_{pore,0}}{K_u}\right)^{\frac{1}{3}} P\ e^{npe}$$

For the interception mechanism correction, the higher values led to an increase in the filtration efficiency for the large particle, as the following equation presents:

$$\eta_R = \eta_{clean,R} 1.5 \left(\frac{\varepsilon_{pore,0}}{K_u}\right)\left(\frac{R^2}{(1+R)^m}\right)$$

After adjusting the previously mentioned parameters, many simulations were carried out to affect the pressure drop and soot loading. Because of many simulations applied, they will be mentioned in the appendix, while the focus will be on presenting the results of two different simulations to explain the difference. The first simulation used the same wall permeability and the default settings for the previous parameters as mentioned in the program guide *Axisuite*. The second simulation was applied after adjusting the wall permeability, and parameters mentioned earlier, as shown in Table 7.

Table 7: Changed parameters for the DPF.

Simulation 1			
Wall loading [g/l]	*Permeability* $[m^2]$	η_D	η_R
0	5e-13	1	1
2.5	5e-13	1	1
Simulation 2			
Wall loading [g/l]	*Permeability* $[m^2]$	η_D	η_R
0	2.5e-14	2	2
2.5	9e-15	2	2

In addition, the soot reaction rate inside the diesel particulate filter was adjusted for the second simulation, as explained in section 5.2.1 down.

5. Result

5.1 DOC

A minimal effect on the pressure drop occurs when exhaust gas passes through the DOC. As mentioned earlier in the DOC section (2.2), it oxidizes both HC and CO and converts them to carbon dioxide and water. In the simulation, the concentrations of HC and CO were not considered. In addition to the above, the DOC oxidizes nitric oxide and converts it to nitrogen dioxide, which helps in better soot oxidation See section 2.2. The results for the NO and NO2 are the same for both simulations. The change in wall permeability and other selected parameters do not affect the result for NO2, NO, as shown below.

5.1.1 NO2

Figure 25 presents the molar fraction of NO2 versus time. The red line is the calculated data from the NOx level as presented in section 4.2.3. The black line presents the result from the simulation. The difference in the results can be observed in the amount of incoming and outgoing NO concentrations, where the outgoing concentrations are higher, which can be explained by reaction (2) inside the DOC.

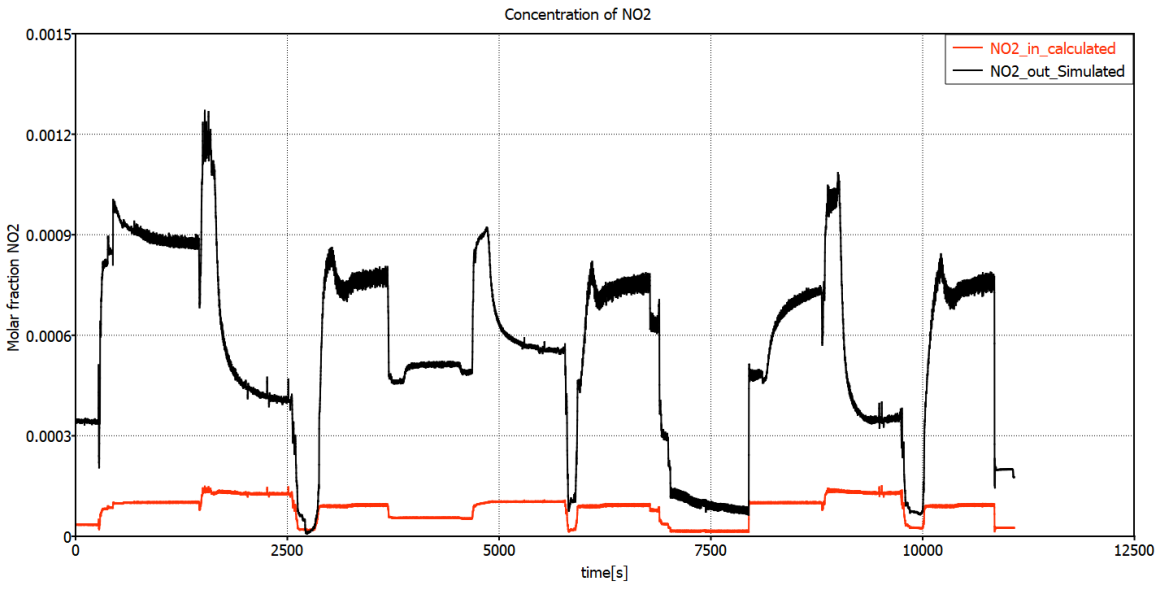

Figure 25: Result of NO2 concentration versus time with calculated NO2 and Simulated for the DOC.

5.1.2 NO

In Figure 26, the calculated NO was used as input, and the result of the simulated NO is plotted versus time. The difference in the values of NO concentration can be explained by the reactions that occur inside the DOC, where nitrogen oxide is formed through the use of NO as an oxidizing agent. See section 2.2

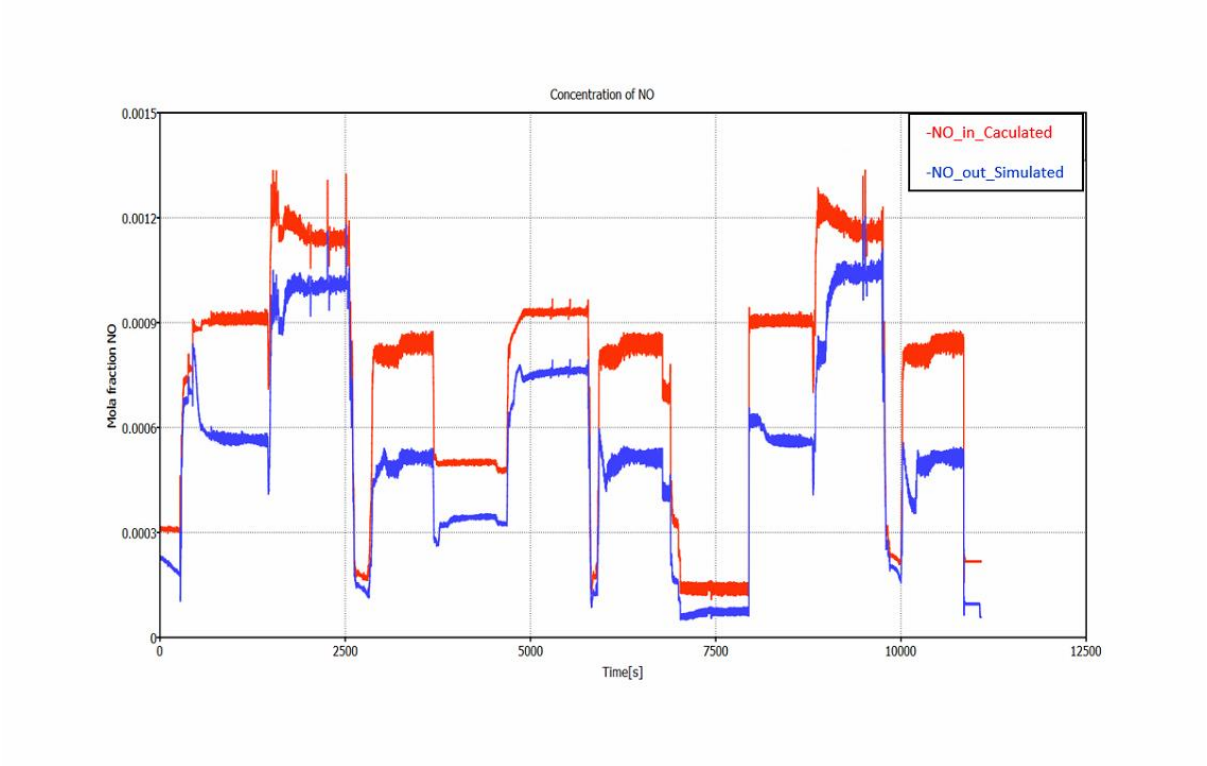

Figure 26: Result of NO concentrations versus time with the calculated concentration of NO (blue line) and the simulated (black line) for the DOC.

5.2 DPF

This section will present the results of a diesel filter in each of the two previously mentioned simulations in section 4.2.6.

5.2.1 Pressure Drop

The pressure drop is one of the most critical factors associated with soot, as the pressure drop increases steadily with the increase in soot formed. Figure 27 presents the first simulation results before adjusting the parameters mentioned in table 7. The results show the incompatibility of the pressure drop between the experimental data and the results resulting from the simulation. The results of the pressure drop from the experiment are higher than the simulation, and therefore there is a more significant amount of soot that managed to cross the filter. The main reason for this is the wall's permeability, which plays an essential role in loading soot into the wall.

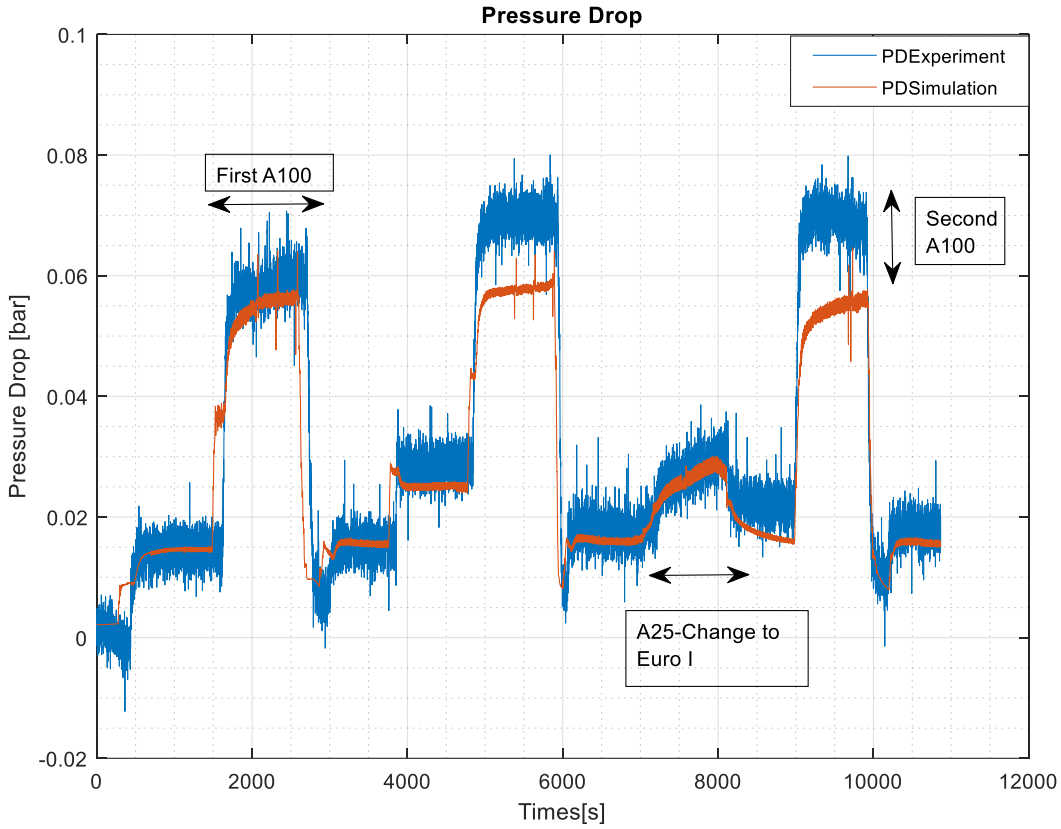

Figure 27: The result for simulated and measured pressure drops versus time for first simulation before change parameter according to Table 7.

From the previous figure, the result for simulated pressure drops increased between the time interval [7111s-8112s] due to a large amount of soot that resulted because of the switch that was made from Euro VI to Euro, I, as shown in Table No 6.

From the exact figure, it can also be noted that the simulation results for the pressure drop when the engine is running at first A100 is more significant than it is at the second point A100. Nevertheless, the engine works under the same conditions Euro VI, i.e., the same speed and load as illustrated in Table No 6.

To verify the reasons for the pressure difference in the two previous regions, the temperature results were first checked. Furthermore, a simulation was carried out by adjusting the temperature used as input in the simulation within a range of $\mp 5℃$. However, there was no change in the simulation results after the temperature modification, as shown in Figure 42 in the appendix.

After checking the measured soot data during the experiment, it was found that the measured amount of soot at the first point was less than the measured amount of soot at the second point, as illustrated in Figure 28.

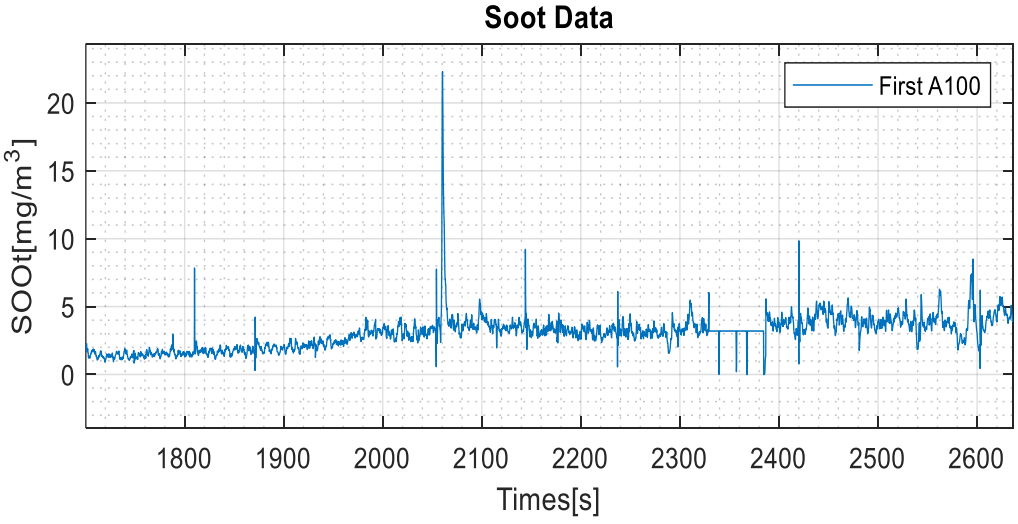

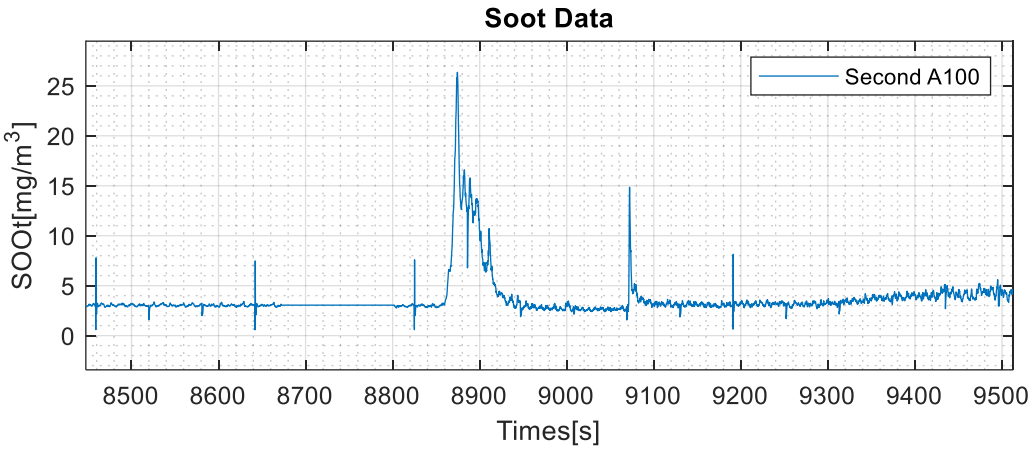

Figure 28: The measured soot data from experiment for the first and second A100.

To improve the soot oxidation to obtain a better pressure drop, the reaction rate was adjusted for reaction No 12 (In section 3.3.1). This was done by adjusting the value of pre-exponential factor A for the soot reactions in the DPF according to the following equation:

$$K = A.e^{-\frac{E}{RT}}$$

Where: A pre-exponential factor, E activation energy.

Modifying the value of the pre-exponential factor A leads to an increase or decrease in the rate of the reaction, as the value of A was modified from $10e^{-4}\ to\ 11e^{-5}$. After adjusting the reaction rate and wall permeability, the results for the second case are presented in Figure 29. The results show a significant difference in the pressure drop compared to the first simulation after adjusting the wall permeability and the correction factor of both the diffusion mechanism and the interception mechanism, which led to better filtering of the transient soot through the DPF, leading to a higher pressure drop.

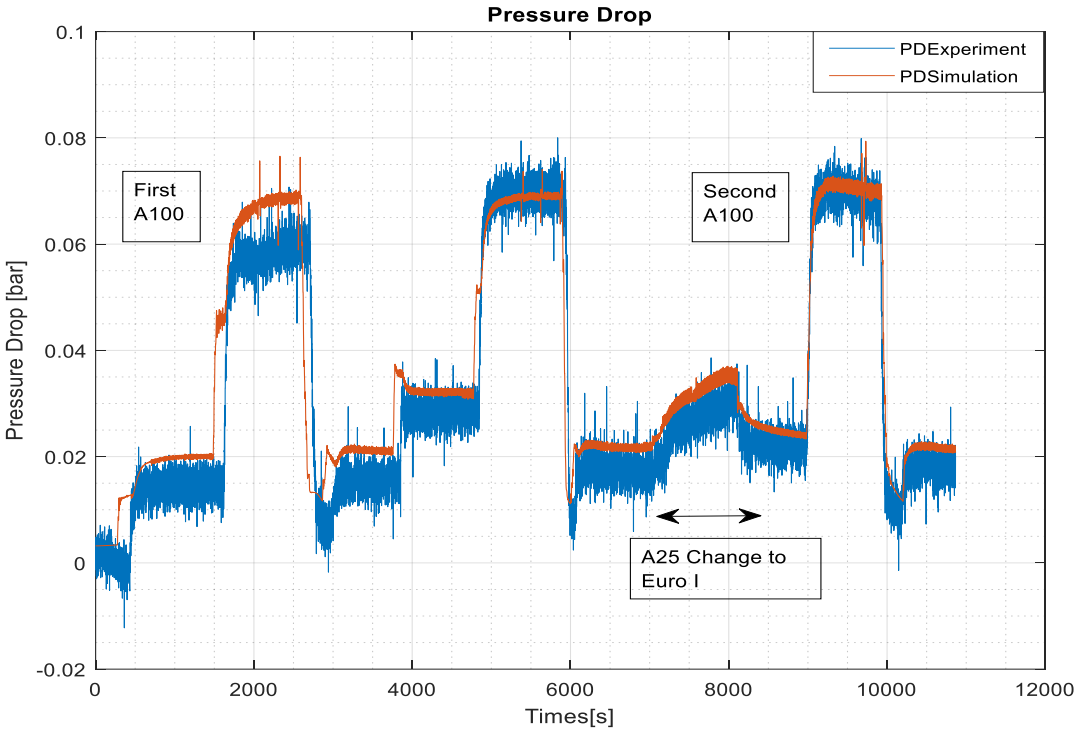

Figure 29: The result for simulated and measured pressure drops versus time for the second simulation after change parameter according to Table 7.

The previous figure shows a good agreement for the pressure drop from the simulation results with the results from the experiment in most points except for the first region, A100, which increase the pressure drop from the experiment.

The reason behind this rise in pressure drop at the first A100 is the higher values in the mass flow rate at the same point, as can be seen in Figure 22a, where the mass flow rate at the first A100 differs by 2.5 % more than from the second A100, and its vast differences affect the result at this point. This difference is due to fluctuations in the engine's work due to the brake system used in the experiment (Water-brake), which sometimes does not guarantee that the engine is stable at the desired point correctly.

Axisuite software relies heavily on mass flow rate to calculate pressure drop and soot concentrations. The high flow rate at the first A100 results in a relatively high-pressure drop at the mentioned point. To confirm the validity of the previous assumption, the mass flow rate was manually reduced by 2% for the first A100. Using the same assumptions for the parameters used in the second simulation, the results showed a pressure drop in correspondence with the data in the studied area without any change in the simulation results for the rest of the points, as explained in Figure 30. This confirms the validity of the analysis of the causes of high-pressure drop for the first A100.

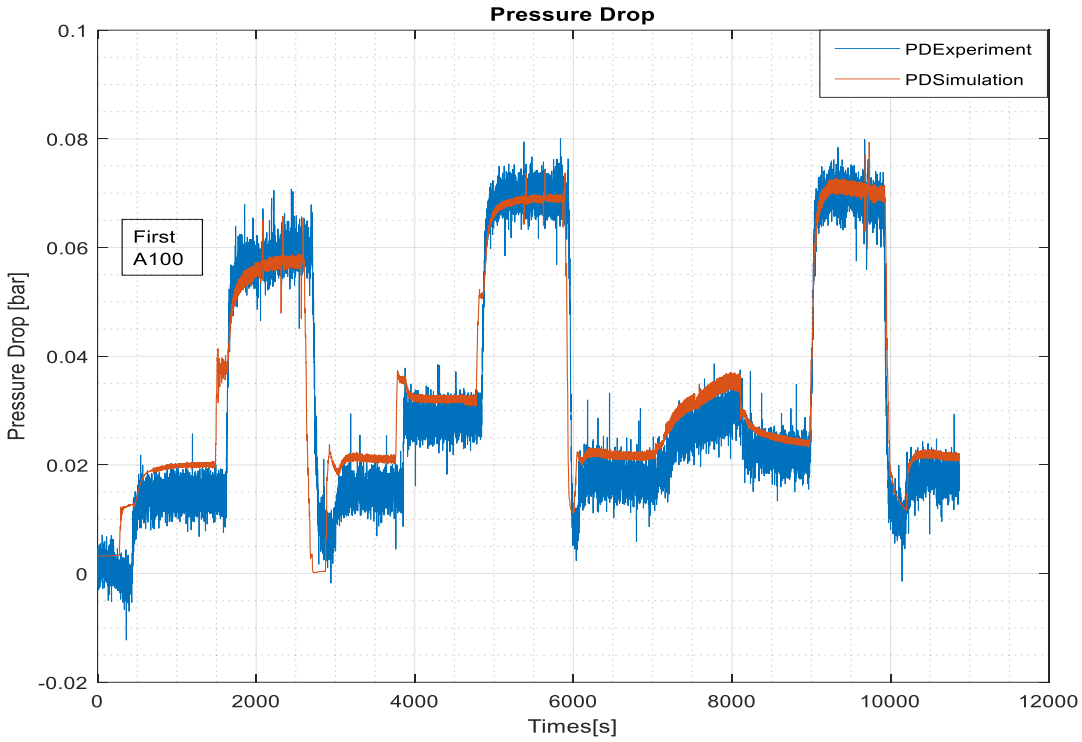

Figure 30: The result for simulated and measured pressure drops versus time after decrease the mass flow rate 2% for the first A100.

5.2.2Temperature

The results for temperatures for the DPF are presented in Figure 31. The black line presents the inlet temperature to the DPF, and the red line shows the outlet temperature for the DPF. The difference in temperatures can be observed, which changes steadily with the engine running. The temperature rises when the engine is running at a high load between the 2000s to 2500s, leading to the combustion of a more significant amount of soot. There is no change in the temperature when the information mentioned in the previous changes. Therefore, in both cases, the results are for the temperatures according to the figure below.

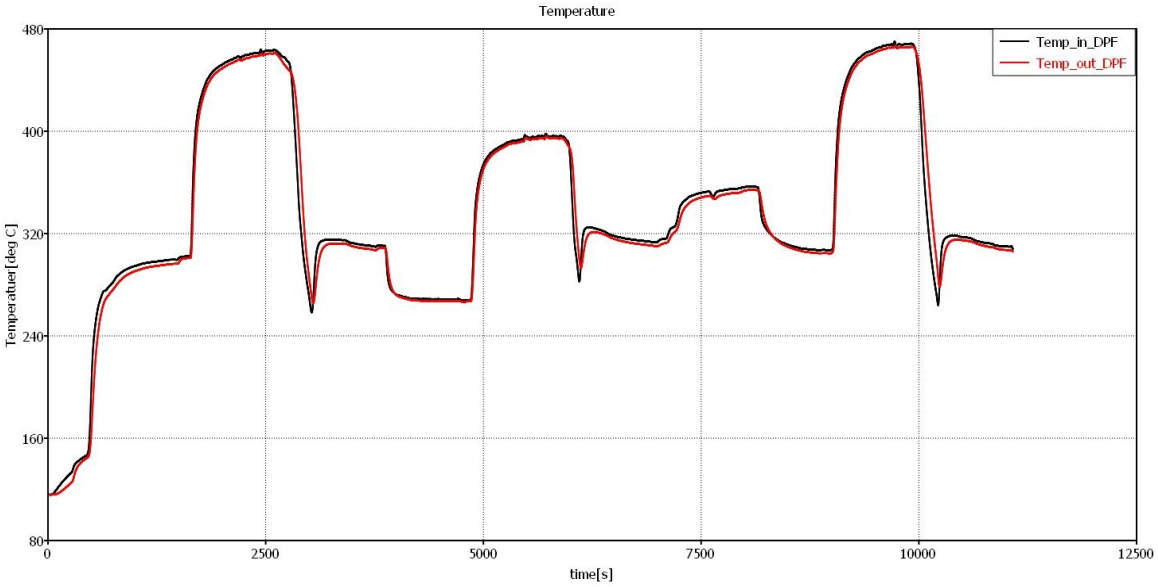

Figure 31: The result for the inlet temperatuer into the DPF versue the outlet temperatuer from the DPF.

5.2.3 Total Soot

The results of the soot concentrations entering and leaving the DOC-DPF for each of the two simulation cases as shown in Figures 32.33.

The first simulation results show the amount of soot coming out of the system without high filtration. This is due to the pressure drop and the wall's permeability in Figure 27. The pressure drop is low, and therefore the amount of soot filtered is less, which in turn leads to a high amount of soot passing through the DPF, as illustrated in Figure 32.

The results for the second show a lower amount of soot coming out of the DPF than in the first simulation, as Figure 33 shows. The main reason for this difference is the wall permeability and the diffusion mechanism correction factor, the intercept permeability correction factor, where the higher wall permeability helps capture a more significant number of particles, thus better filtration of soot. Also, the diffusion mechanism correction factor and the interception mechanism correction factor, the larger values mentioned in the table, help increase the filtering efficiency of both small and large particles.

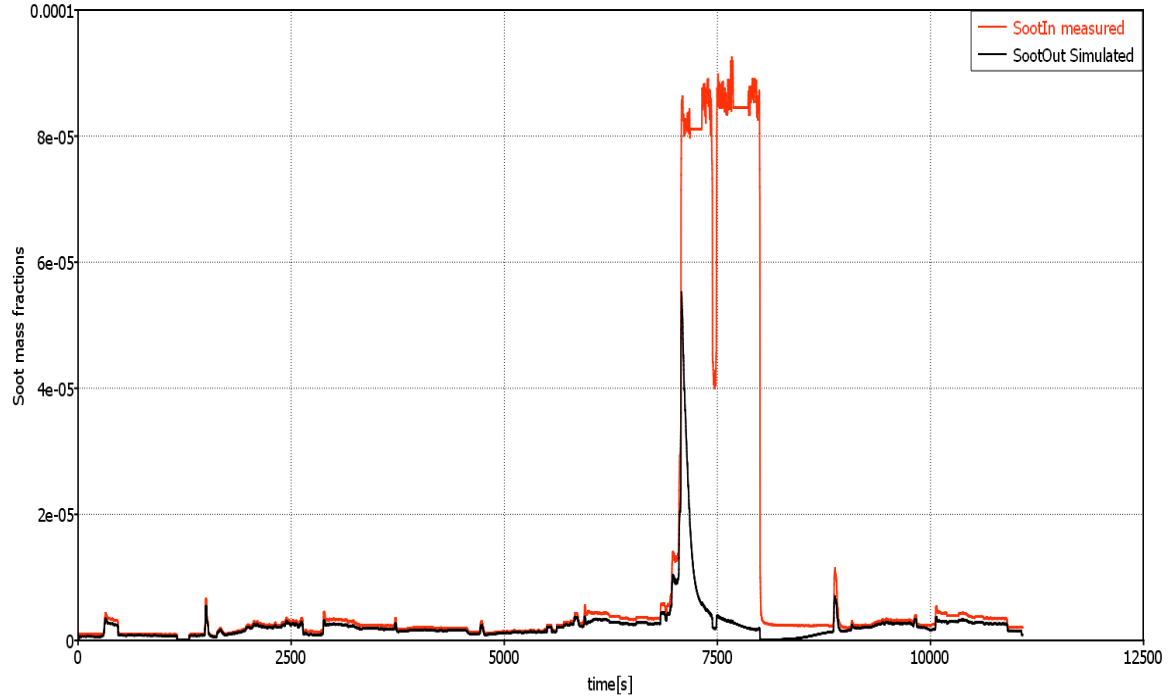

Figure 32: The result for the soot measured versus the soot simulated for the model DOC-DPF before change the parameters.

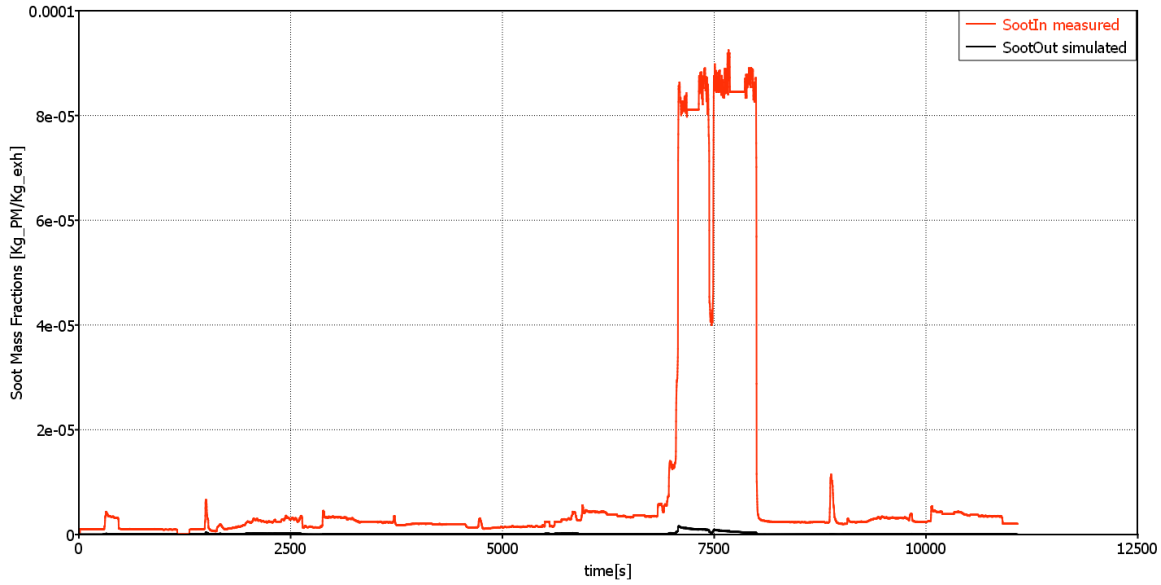

Figure 33: The result for the soot measured versus the soot simulated for the model DOC-DPF after change the parameters.

5.2.4 Soot loading

The results for loading soot show the difference between the amount of soot filtered when the soot exhaust gas passed through the DFP.

The results for the first simulation are as shown in Figure 34. The results show the total amount of soot that was filtered, which amounts to 3.4 $\left[\frac{g}{l}\right]$. Soot filtration is directly related to the decrease in pressure, as an increase leads to better filtering of soot due to the weak pressure drop, as presented in Figure No. 27. Higher soot loading means better filtration inside the DPF. To clarify the difference in soot loading between the two studied cases, the amount of filtered soot was read for each A100.

Figure 35 presents the simulation results for the second case, where the total amount of filtered soot increased, which amounts to 4.27 $[\frac{g}{l}]$. The main reason behind this improvement is the increase in pressure drop due to the modification of the wall permeability and the improvement of the previously mentioned information. By looking at the same points, it can be noted that the amount of soot filtered increased at the first point, A100, and for the second point, as shown below.

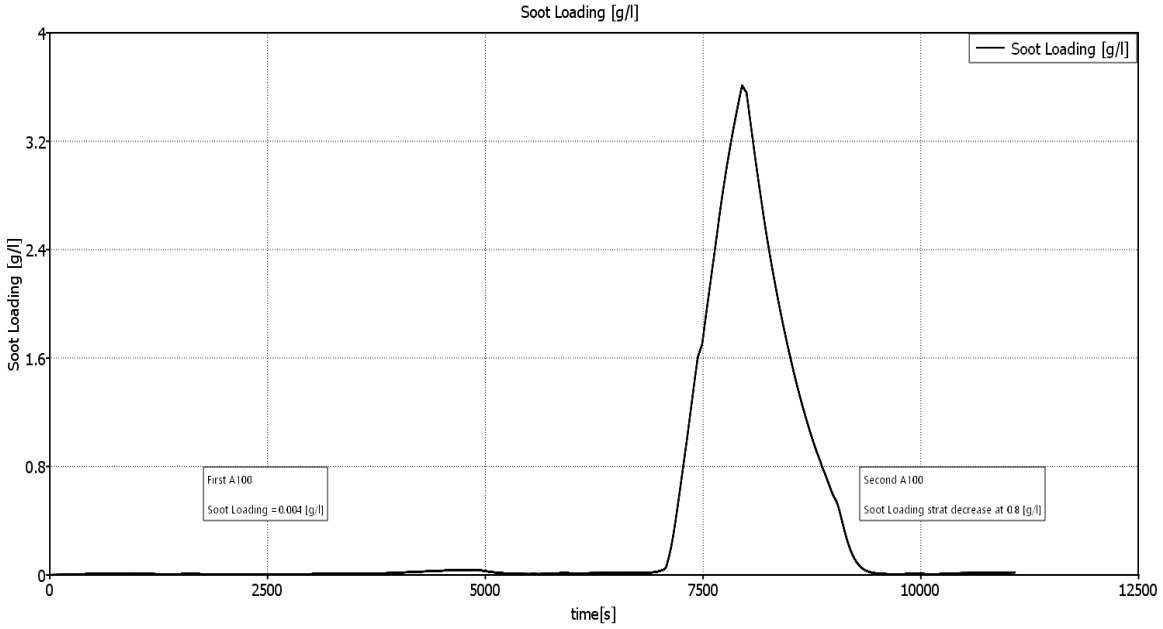

Figure 34: The result for the Soot loading inside the DPF for the first simulation.

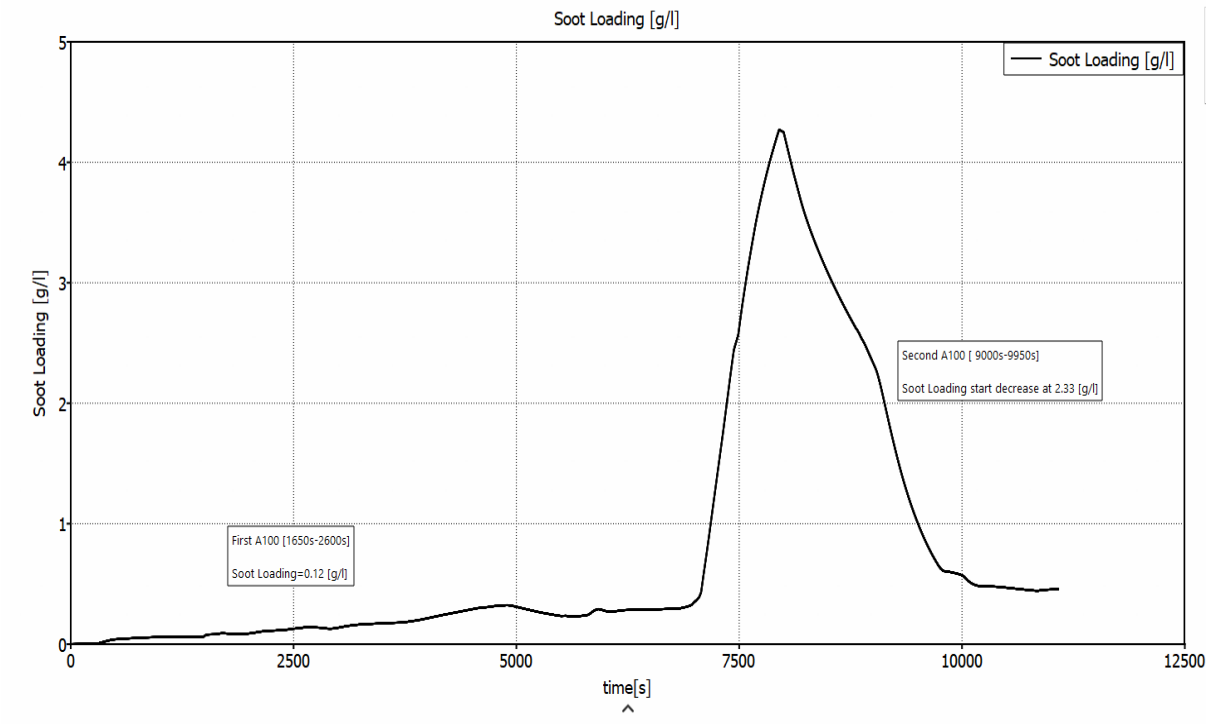

Figure 35: The result for the Soot loading inside the DPF for the second simulation.

5.2.5 Filtration efficiency

The efficiency of filtration was studied during different periods selected consistently at time points in which the pressure drops and, therefore, the amount of filtered soot varies. The filtration efficiency is calculated based on the soot distribution and particle size d. The particle size calculation is depended on the algorithm used in the *Axisuite*. Since the normal soot distribution was used with number particle class 10 (realistic), the particle size was not measured during the experiments. Therefore, there is no particle size data to compare with the simulation results.

When the particle diameter increases, there is a decrease in filtration efficiency, leading to an increase in pressure drop. To raise the filtration efficiency, higher values should be used for each diffusion mechanism, which helps raise the filtering mechanism of small particles. In contrast, the intercept mechanism helps to increase the efficiency of filtering large particles.

The filtering efficiency results for both simulations were selected at the points concerning the engine test cycle as follows:

Table 8: Selected points for filtration efficiency

A25	A100	C25	C50	C75	A100
1000s	2100s	3500s	4500s	5500s	95000s

Figure 36 represents the result for the first simulation; the results show that the filtration efficiency decreases in all the studied points with the increase in the diameter of the particles. However, there is a difference in the percentage of filtration efficiency among the studied points. For example, the filtration efficiency decreases at point C25 from 72 % to 14 %, while the filtration efficiency of point C50 decreases from 65% to 22%.

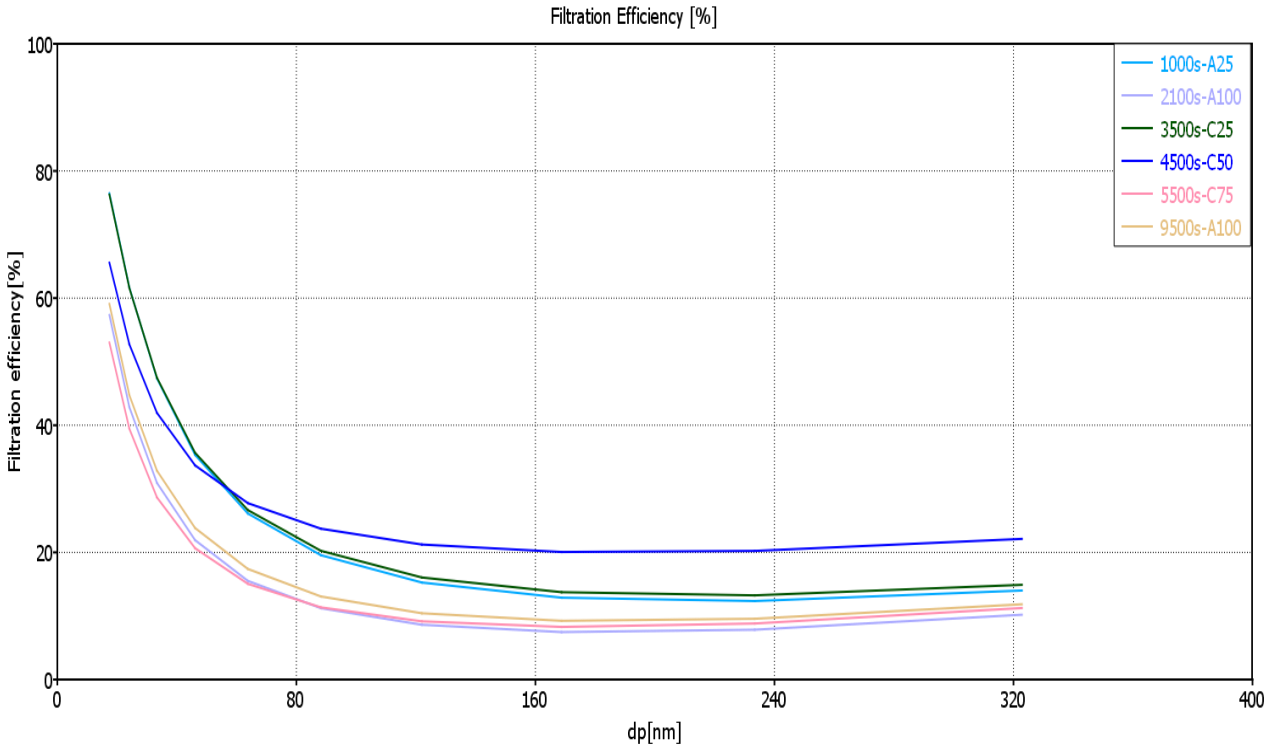

Figure 36: The result for filtration efficiency per particle size for first simulation

The difference in the filtration efficiency of the two mentioned points is due to the difference in particle size concentration, as Plotted in Figure 37. The capture efficiency as presented in the equations below depends on both size and amount of soot, and when the particle size is less than 100 nm, the Brownian diffusion dominates ,when the size is more than 1μm, the inertial forces dominate.[30]

$$CE = \frac{PM_{in} - PM_{out}}{PM_{in}}$$

Soot concentrations and amount with smaller diameter are greater for point C25 than point C50, soot concentration with large particle size is higher for C25 than C50. As a result, the filtration efficiency is higher when the soot amount and the number of particles of smaller diameter is higher, and this explains the reason why the filtration efficiency starts for C25 at 79% while C50 starts at 65%. As mentioned above, the filtration efficiency decreases with the increase in the size of the particles, and due to the higher

soot concentration with large particle size for C25, the efficiency decreases to 14 % compared to C50, which decreases to 22% because of the lower amount of soot concentration with large particle diameter.

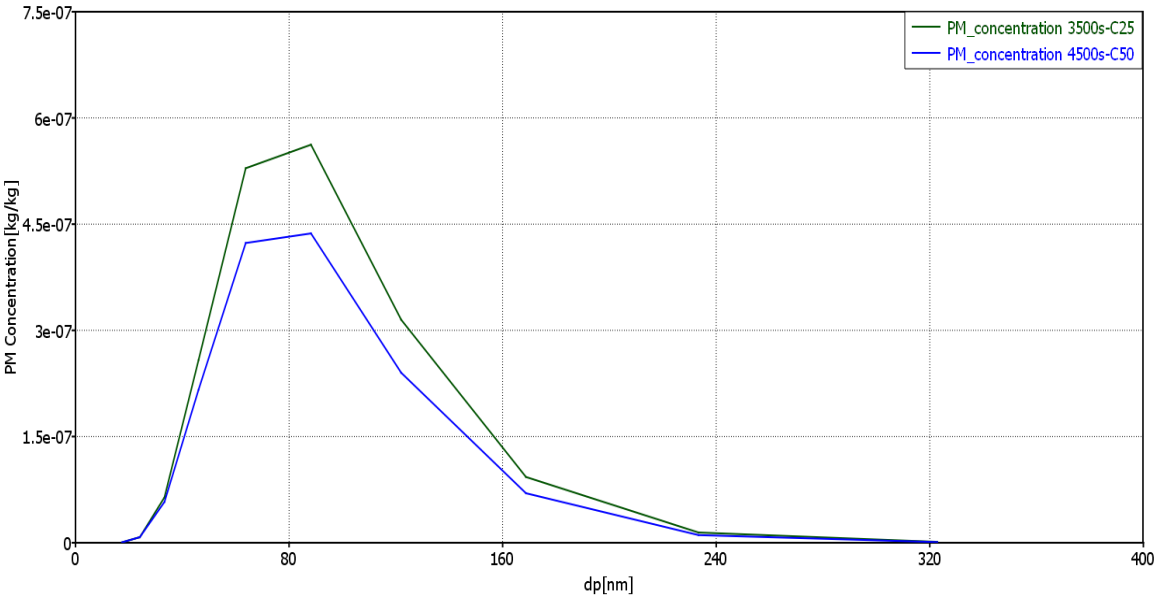

Figure 37: The result for PM Concentration for points (C25-C50) versus particle size.

The result for the second simulation for the same sleeted points is plotted in Figure 38. The results clarify that the filtration efficiency increased by up to 40% compared to the filtration efficiency of the first case. The difference in the filtration efficiency is due to the same reason as explained above. The change in the value of the diffusion and interception correction mechanism leads to better filtration efficiency, as shown in the figure below, which leads to an increase in the amount of soot that is filtered while passing through the DPF.

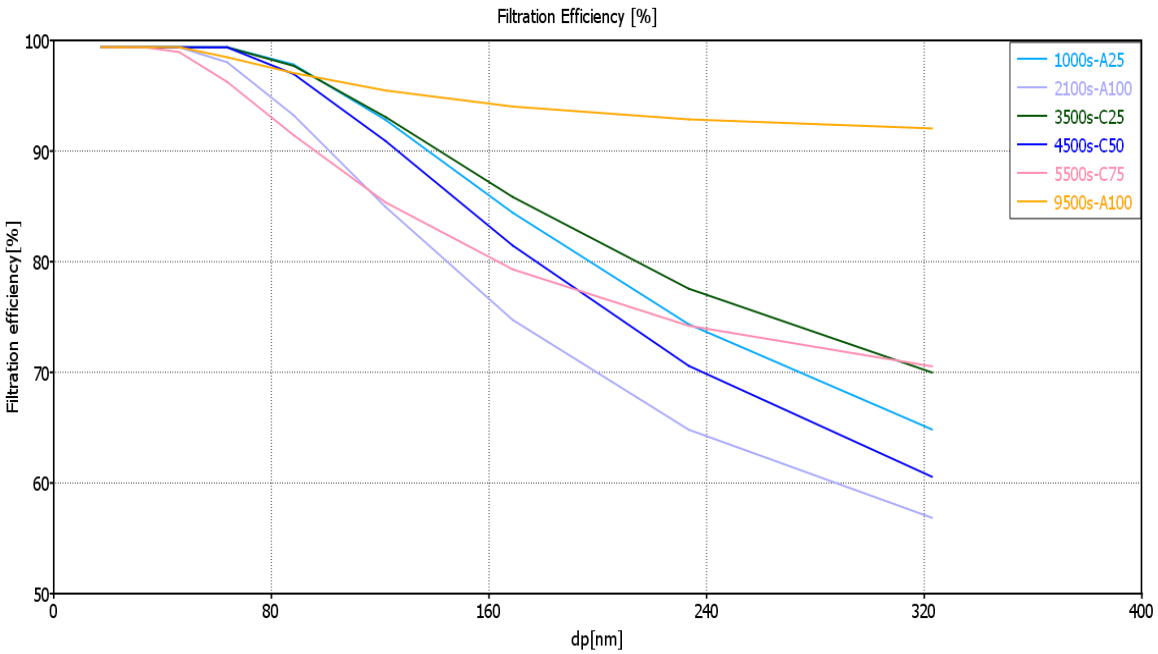

Figure 38: The result for filtration efficiency per particle size for the second simulation.

5.2.6 PM concentration

The results for the particle mass concentrations distributed on the monolith's surface are plotted in a 3D graph to show the particle concentration on the surface versus time for different particle sizes. Since the soot log-normal distribution was used and the number of particle classes selected to 10 (realistic), the data for particle size was not measured during the experiment. Plotting particle mass concentrations helped know the amount of incoming and outgoing soot before and after adjusting the previously mentioned parameters. Figure 39 shows the soot particle mass concentration; the blue axis represents the soot concentration, the red axis presents the number of particle classes, and the green axis shows the simulation time.

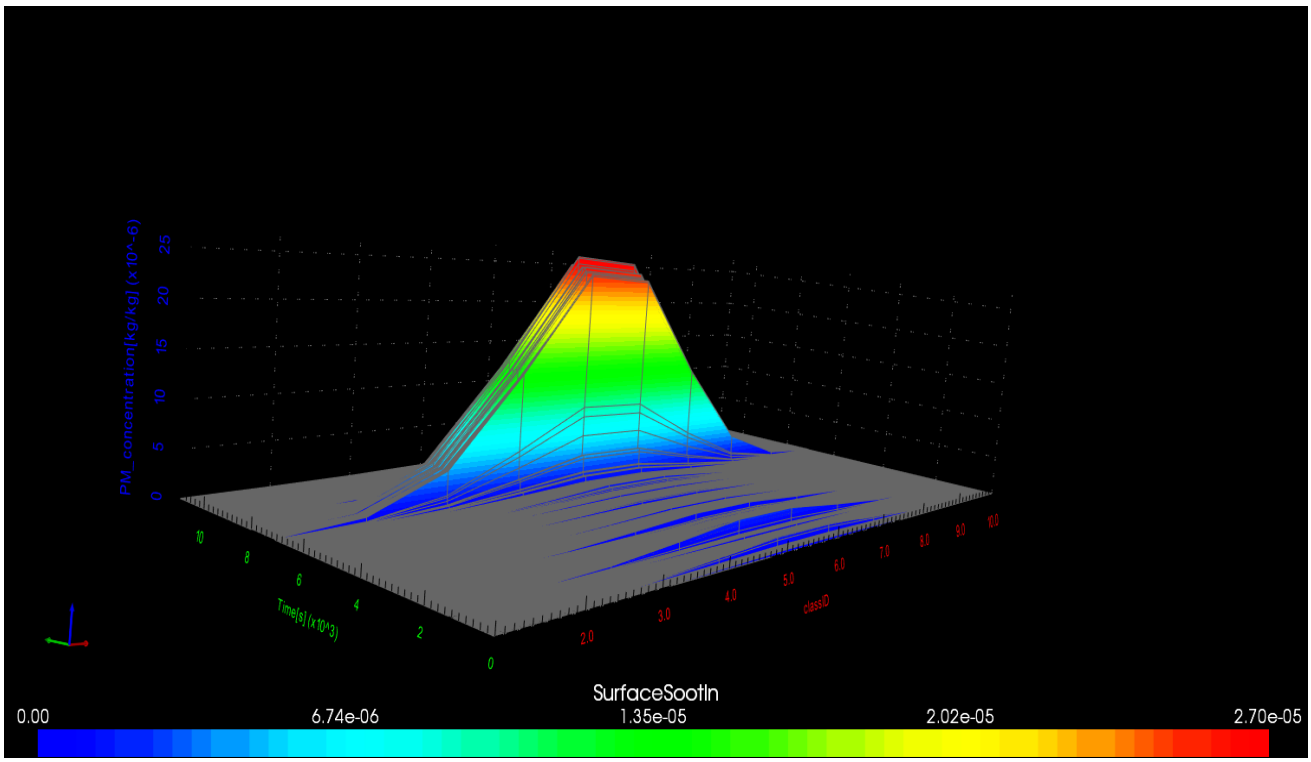

Figure 39: PM concentration in (blue axis) versus number pf particle classes (red) and simulation time.

The results for soot mass concentration for the first simulation before adjusting wall permeability and other parameters, as shown in Table 7, are plotted in Figure 40. From the results, it is clarified that the soot concentrations (the blue axis) decreased by 50% compared to the amount of soot entering. Therefore, about half of the soot was filtered through the diesel particulate filter.

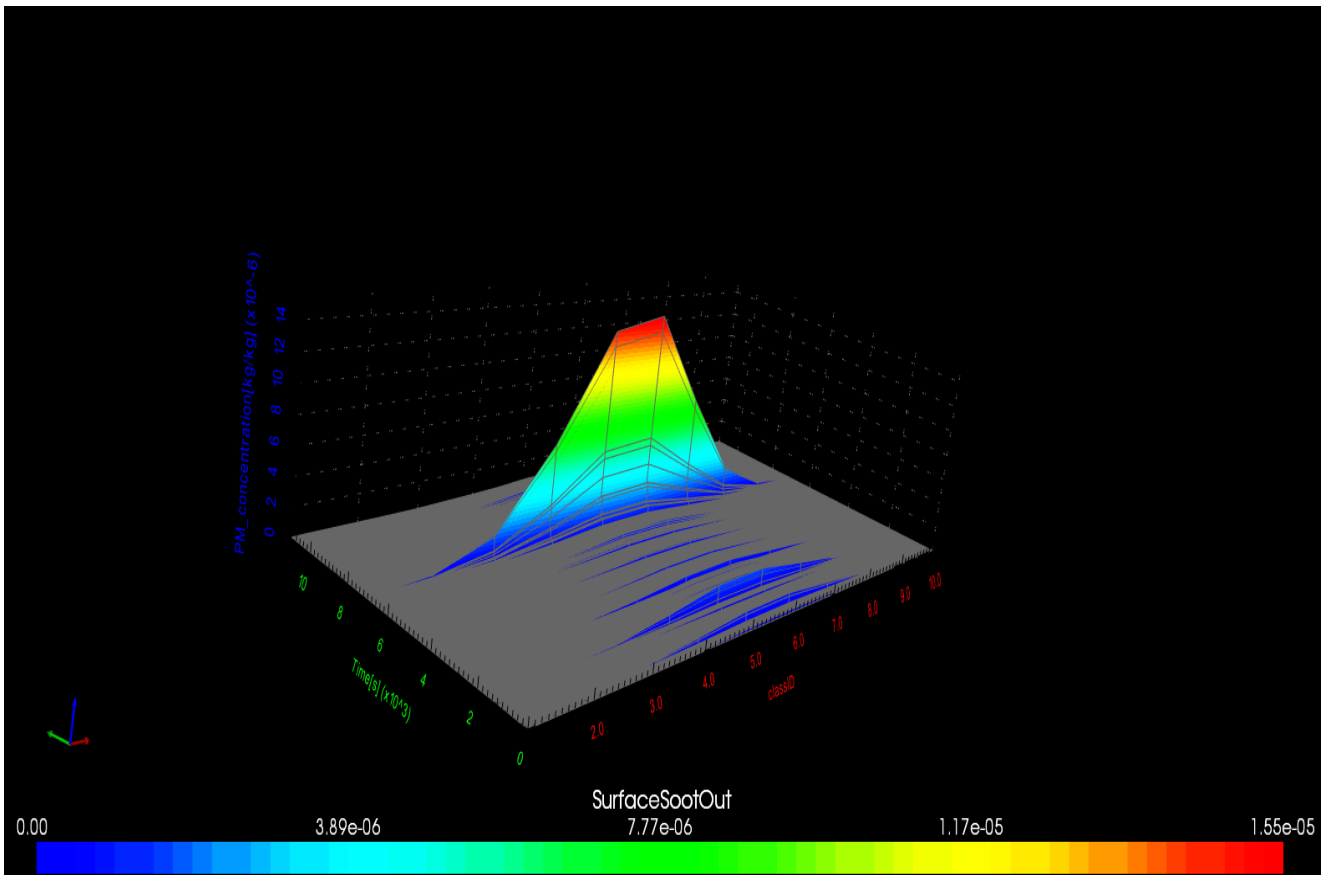

Figure 40: The result for PM concentration out (blue axis) versus number of particle classes (red) and simulation time before adjusting the parameters (Simulation 1).

Figure 41 plotted the result for soot concentration for the second simulation after changing the wall permeability and diffusion and interception correction mechanisms. The result clarifies that the amount of soot mass coding has decreased by up to 95% compared to the amount of incoming soot that ranged between $0{:}\,25\ e^{-06}[\frac{kg}{kg}]$ In contrast, quantities of soot mass for the second simulation are $0{:}\,5e^{-06}[\frac{kg}{kg}]$ as potted in the figure below.

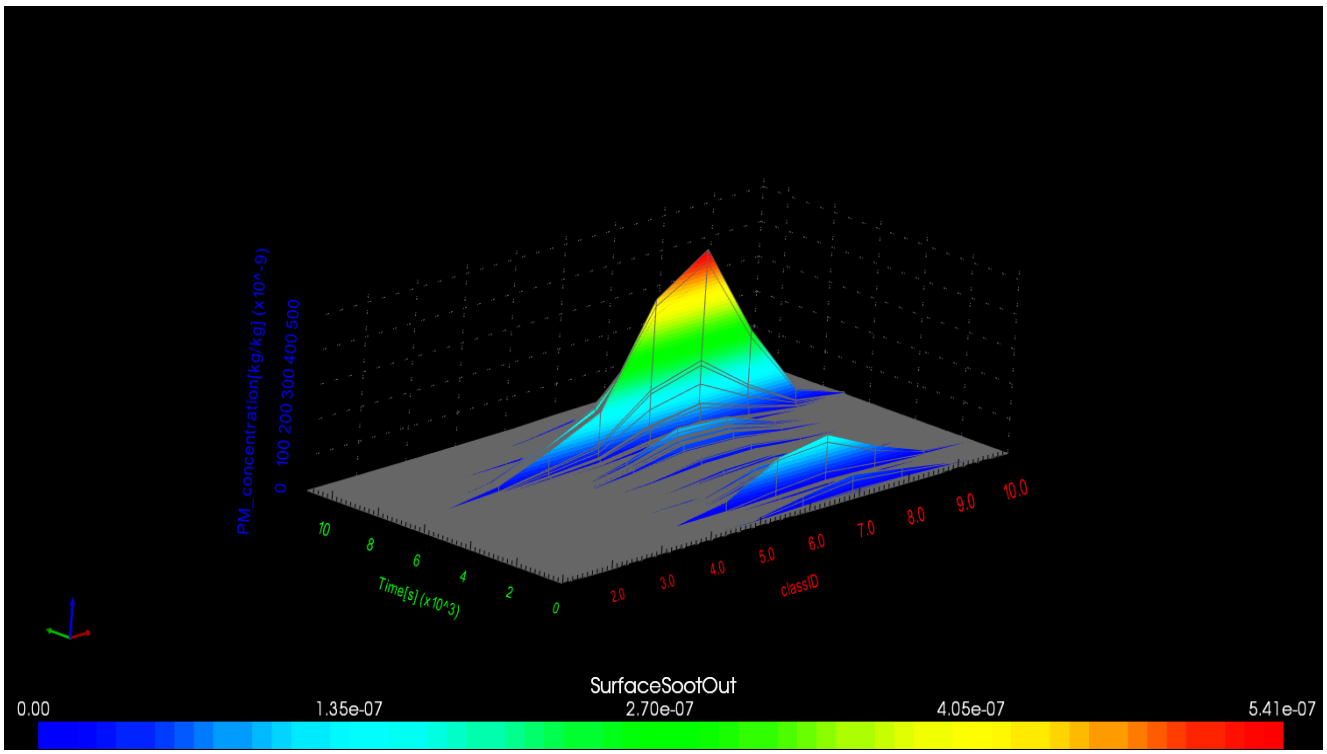

Figure 41: The result for PM concentration out (blue axis) versus number of particle classes (red) and simulation time after adjusting the parameters (Simulation 2).

6. Summary and Conclusion

The inconsistency of the simulation results for pressure drop with the experimental data is one of the most critical problems that need to be focused on for a better study of soot filtration. This thesis mainly focused on studying the parameters that lead to improving the pressure drop in line with the experimental data and studying the results and their impact on soot loading.

The focus was on the following parameters: wall permeability, diffusion mechanism correction, interception mechanism correction, and soot reaction speed within the DPF which had a significant impact in improving the simulation results significantly to match the experimental data.

The results showed the incompatibility of the pressure drop between the first simulation and the experimental data, as one-diameter wall permeability (inlet-outlet) was used, as shown in Figure 27. The filtration efficiency ratio was low, and the first simulation results ranged between 70%-14%. The same is true for loading soot, as the soot filtration rate did not exceed 50%, leading to the passage of many particles without filtering.

The second simulation results after adjusting the permeability of the wall, the diffusion correction mechanism, the interception correction mechanism, and the reaction speed showed a significant agreement of the pressure drop results from the simulation with the experimental pressure drop data, as shown in Figure 29. The results also showed the importance of measuring the mass flow rate and its effect on the pressure drop results, as shown in Figure 30. The results of loading soot significantly improved, as shown in Figure 35, compared to the first simulation, where the percentage reached 95%. The filtration efficiency increased by 40%, ranging between 100%-60%, thus better soot filtration.

7. Future work

More experiments should be conducted for future work, and the experimental measurements must be validated. More research should be considered on the effect of wall permeability and other parameters because of its positive effect on the increase of filtered soot amounts in the DPF, experimenting with different types of filters with different sizes. In addition, optimizing different parameters by calculating the error rate because the relatively long simulation time of 3:20 hours did not calculate the error rate and adjust the parameters, so there is a need for more calibration for the different parameters by calculating the error rate and trying to improve it.

8. Reference

[1] VolvoTrucks, "One-Box Aftertreatment " Online vol. 2, 2022/06/02. [Online]. Available: https://www.volvotrucks.us/trucks/emissions/.

[2] İ. A. Reşitoğlu, K. Altinişik, and A. Keskin, "The pollutant emissions from diesel-engine vehicles and exhaust aftertreatment systems," *Clean Technologies and Environmental Policy,* vol. 17, no. 1, pp. 15-27, 2015.

[3] R. Prasad and V. R. Bella, "A review on diesel soot emission, its effect and control," *Bulletin of Chemical Reaction Engineering & Catalysis,* vol. 5, no. 2, p. 69, 2010.

[4] P. Aakko-Saksa, P. Roslund, and P. Koponen, *Development and validation of comprehensive emission measurement methods for alternative fuels at VTT*. 2017.

[5] L. Tang *et al.*, "The impact of ship emissions on air quality and human health in the Gothenburg area–Part 1: 2012 emissions," *Atmospheric Chemistry and Physics,* vol. 20, no. 12, pp. 7509-7530, 2020.

[6] W. A. Majewski and H. Jääskeläinen, "Exhaust particulate matter," *Dieselnet. Retrieved,* vol. 6, p. 2021, 2019.

[7] DieselNet, "EU: Heavy-Duty Truck and Bus Engines," Online vol. 6, 2022. [Online]. Available: https://dieselnet.com/standards/eu/hd.php.

[8] M. K. Khair and H. Jääskeläinen, "Exhaust gas recirculation," *DieselNet Technology Guide. Disponível em: https://www. dieselnet. com/tech/engine_egr_sys. php. Acesso em,* vol. 3, 2006.

[9] W. A. Majewski, "Selective catalytic reduction," *Ecopoint Inc. Revision,* Online vol. 6, 2005. [Online]. Available: https://dieselnet.com/tech/cat_scr.php.

[10] B. R. Gurjar, L. T. Molina, C. S. P. Ojha, and C. S. P. Ojha, *Air Pollution : Health and Environmental Impacts*. Baton Rouge, UNITED STATES: Taylor & Francis Group, 2010.

[11] O. Velentza, "Particular matters: a threat for human health," *Αιωρούμενα σωματίδια: μια απειλή για την υγεία του ανθρώπου,* Article vol. 21, no. 3, pp. 233-244, 2016. [Online]. Available: https://search.ebscohost.com/login.aspx?direct=true&AuthType=sso&db=bsu&AN=122021447&site=ehost-live&scope=site&authtype=sso&custid=s3911979.

[12] W. A. Majewski, "Catalytic Diesel Filters," 2020. [Online]. Available: https://dieselnet.com/tech/dpf_catalytic.php.

[13] W. H. Organization and W. E. C. f. Environment, *WHO global air quality guidelines: particulate matter (PM2. 5 and PM10), ozone, nitrogen dioxide, sulfur dioxide and carbon monoxide*. World Health Organization, 2021.

[14] S. DieselNet, "Emission Standards, European Union, Heavy-Duty Diesel Truck and Bus Engines," ed, 2009.

[15] Naturvardsverket, "Utsläpp till luft," p. Svenska, 1990/2020. [Online]. Available: https://www.naturvardsverket.se/data-och-statistik/luft/utslapp.

[16] H. Jääskeläinen and M. K. Khair, "EGR systems and components," *DieselNet Technology Guide, https://www. dieselnet. com/tg,* 2012.

[17] M. K. K. Hannu Jääskeläinen, "Effect of EGR on Emissions and Engine Performance," 2017. [Online]. Available: https://dieselnet.com/tech/engine_egr_emissions.php.

[18] M. W. Addy, "Diesel particulate filter," *Dieselnet, https://www. dieselnet. com/tech/dpf. php,* 2011.

[19] W. A. Majewski, "Diesel Filter Regeneration," *DieselNet Technology Guide. Ecopoint Inc,* 2005.
[20] W. A. Majewski, "PhD" Diesel Oxidation Catalyst," *Diesel Net Technology Guide,* 2021. [Online]. Available: https://dieselnet.com/tech/cat_doc.php.
[21] J. H. Johnson, S. T. Bagley, L. D. Gratz, and D. G. Leddy, "A Review of Diesel Particulate Control Technology and Emissions Effects - 1992 Horning Memorial Award Lecture," 1994. [Online]. Available: https://doi.org/10.4271/940233.
[22] W. A. Majewski, "Selective catalytic reduction," *Ecopoint Inc. Revision,* 2005.
[23] M. K. Khair and W. A. Majewski, "Diesel emissions and their control," SAE Technical Paper, 2006.
[24] OTOMATIC, "DPF structure," 2022. [Online]. Available: https://www.otomatic.co.uk/dpf-structure/.
[25] C. Depcik, B. Spickler, and A. Gaire, "Revisiting the Single Equation Pressure Drop Model for Particulate Filters," *SAE International Journal of Engines,* vol. 11, no. 6, pp. 1421-1446, 2018, doi: https://doi.org/10.4271/2018-01-0952.
[26] DieselNet, "Nonroad Transient Cycle (NRTC)," 2022. [Online]. Available: https://dieselnet.com/standards/cycles/nrtc.php.
[27] DieselNet, "European Stationary Cycle (ESC)," 2022. [Online]. Available: https://dieselnet.com/standards/cycles/esc.php.
[28] L. J. Clapp and M. E. Jenkin, "Analysis of the relationship between ambient levels of O3, NO2 and NO as a function of NOx in the UK," *Atmospheric Environment,* vol. 35, no. 36, pp. 6391-6405, 2001.
[29] "
MSSplus - AVL Micro Soot Sensor," *AVL* 2022. [Online]. Available: https://www.avl.com/-/mssplus-avl-micro-soot-sensor.
[30] J. Sjöblom and H. Ström, "Capture of Automotive Particulate Matter in Open Substrates," *Industrial & Engineering Chemistry Research,* vol. 52, pp. 8373-8385, 06/26 2013, doi: 10.1021/ie4004333.

Appendix

Appendix 1 Terminology

ρ	$Density\ [kg/m^3]$
v	$Gas\ velocity\ [\frac{m^2}{s}]$
N	$Number\ of\ permeable\ sides$
ρ_w	$Density\ of\ deposit\ inside\ the\ wall\ [\frac{kg}{m^3}]$
v_w	$velocity\ of\ deposit\ inside\ the\ wall\ [\frac{m^2}{s}]$
α	$thermal\ diffusivity\ [\frac{m^2}{s}]$
d	$Hydraulic\ diamter\ of\ a\ clean\ channel\ [m]$
μ	$Dynamic\ viscosity\ [Pa.s]$
c_4	$Slip\ correction\ factor\ [\frac{ms}{(\text{kg moleT})^{0,5}}]$
V_{trap}	$Effective\ trap\ Volume\ [m^3]$
w_w	$Substrate\ wall\ thickness\ [m]$
w_p	$Soot\ Layer\ thickness\ [m]$
T	$Temperature\ [K]$
$\Re$	$Gas\ constant\ [\frac{J}{molK}]$
ξ	$Additive\ concentration\ in\ deposit\ Layer$
d_h	$Hydraukic\ diameter\ of\ a\ channel[m]$
H	$Heat\ source\ component\ [\frac{w}{m^3}]$

l	$Channel\ length\ [m]$
C_p	$Specific\ heat\ capacity\ [\frac{J}{KgK}]$
λ	$Thermal\ conductivity\ [\frac{W}{mK}]$
S	$Heat\ soure\ term\ [\frac{W}{m^3}]$
v	$exhaust\ gas\ velocity\ [\frac{m}{s}]$
H_{react}	$Reaction\ heat\ \left[\frac{J}{mol}\right]$
d	$Hydraukic\ diameter\ of\ a\ channel[m]$
$\sum R'_k$	$Total\ of\ all\ soot\ oxidation\ reaction\ rates$
E	$Filtration\ Efficiency$
μ_p	$Concentration\ of\ soot\ particles$
m_{NOx}	$The\ NOx\ mass\ flow\ rate\ \left[\frac{g}{s}\right]$
MW_{NOx}	$The\ molecular\ weight\ of\ the\ NOx\ \left[\frac{mol_{NOx}}{g}\right]$
$m_{exhaust}$	$The\ exhaust\ gas\ mass\ flow\ rate\ \left[\frac{g}{s}\right]$
$MW_{exhaust}$	$The\ exhaust\ gas\ molecular\ weight\ [\frac{mol_{exhaust}}{g}]$
D_{part}	$The\ particle\ diffusivity$
$\varepsilon_{pore,0}$	$The\ pore\ volume\ fraction$
d_{pore}	$The\ mean\ pore\ size$

Appendix 2 Result

PREEM AB
Certificate of Quality

Specification	**SD-DIESEL MK1 LC**	Sampling Date	**2021-05-12**
Nomination Number	**ITS40-1-235**	Delivery Date	
Sample Number	**GO21-05267-01**	Reference No	
Sample Site	**DSPBITS40**	Comment	

Diesel MK1, w/o FAME, item no. 235,4235

Properties	Results	Units	Ref. Test Methods
Appearance at 20°C	C&B	Visual	Visual inspection
Appearance at 20°C	1	rating	ASTM D4176
Aromatic content	4,9	% V/V	SS 15 51 16
Ash content	<0,010	% m/m	SS-EN ISO 6245
Carbon content	86,2	% m/m	ASTM D 5291
Carbon Hydrogen ratio	5,94	% m/m	Calculated
Carbon residue (on 10% dist res)	<0,20	% m/m	SS-EN ISO 10370
Cetane index	53,2		SS-EN ISO 4264
Cetane number	55,8		SS-EN ISO 5165
Cloud point	-34	°C	SS-EN ISO 3015
Cold Filter Plugging Point	-35	°C	SS-EN 116
Colour (ASTM scale)	L0,5		SS-ISO 2049
Conductivity at 20°C	360	pS/m	SS-ISO 6297
Cu strip corrosion (3h at 50°C)	class 1	Rating	SS-EN ISO 2160
Density at 15°C	814,0	kg/m³	SS-EN ISO 12185
Dist: IBP	182,0	°C	SS-EN ISO 3405
Dist: Temp. at 10% V/V rec.	206,6	°C	SS-EN ISO 3405
Dist: Temp. at 50% V/V rec.	235,0	°C	SS-EN ISO 3405
Dist: Temp. at 90% V/V rec.	275,3	°C	SS-EN ISO 3405
Dist: Temp. at 95% V/V rec.	283,6	°C	SS-EN ISO 3405
FAME content	<0,1	% V/V	SS-EN 14078
Flash point	72,0	°C	SS-EN ISO 2719
Hydrogen content	14,5	% m/m	ASTM D 5291
Lubricity (WSD) at 60°C, Method A	250	µm	SS-EN ISO 12156-1
Manganese content	<2,0	mg/l	SS-EN 16576
Net heat of combustion	43,388	MJ/kg	ASTM D 4809
Oxygen content	<0,1	% m/m	Calculated
Oxidation stability	<25	g/m³	SS-EN ISO 12205
PAH content	0,02	% V/V	SS 15 51 16
Sulphur content	<5,0	mg/kg	SS-EN ISO 20884
Total contamination	<24,0	mg/kg	SS-EN 12662
Viscosity at 40°C	1,998	mm²/s	SS-EN ISO 3104
Water content	<30	mg/kg	SS-EN ISO 12937

Figure 42: The certificate of quality PREEM

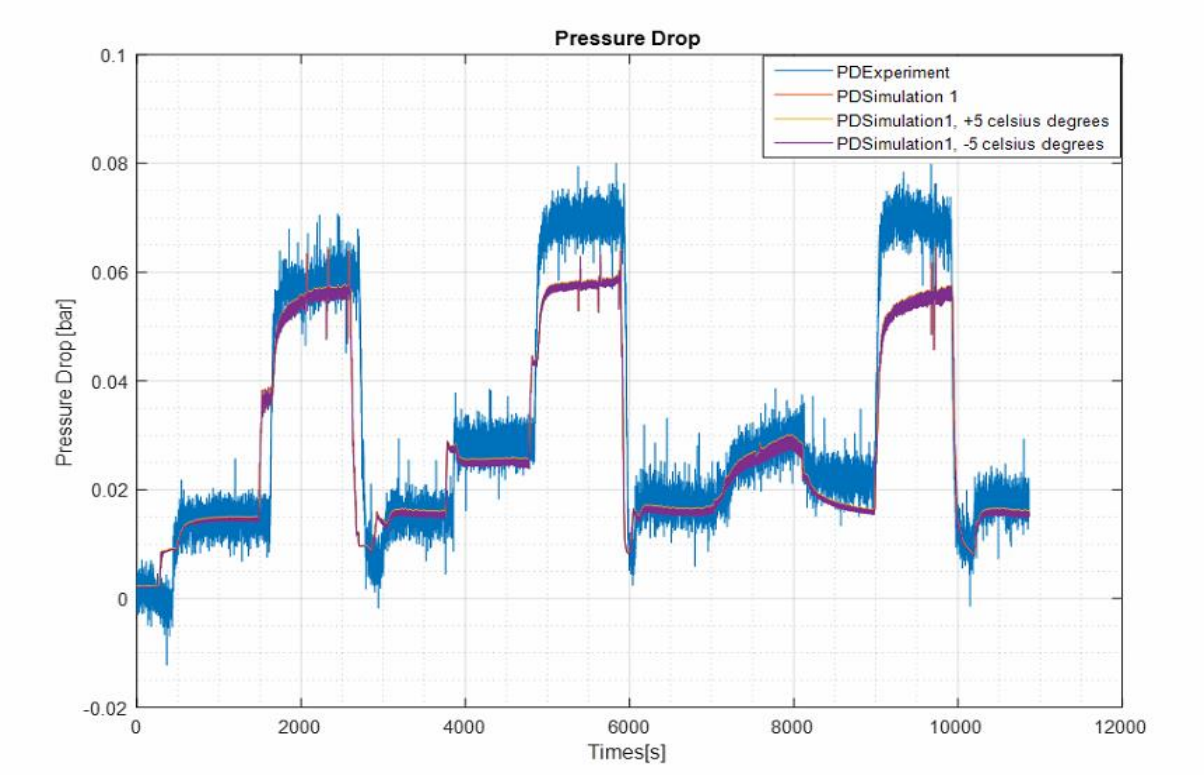

Figure 43: The result for pressure drops versus time after adjusting the temperature with range ∓ 5

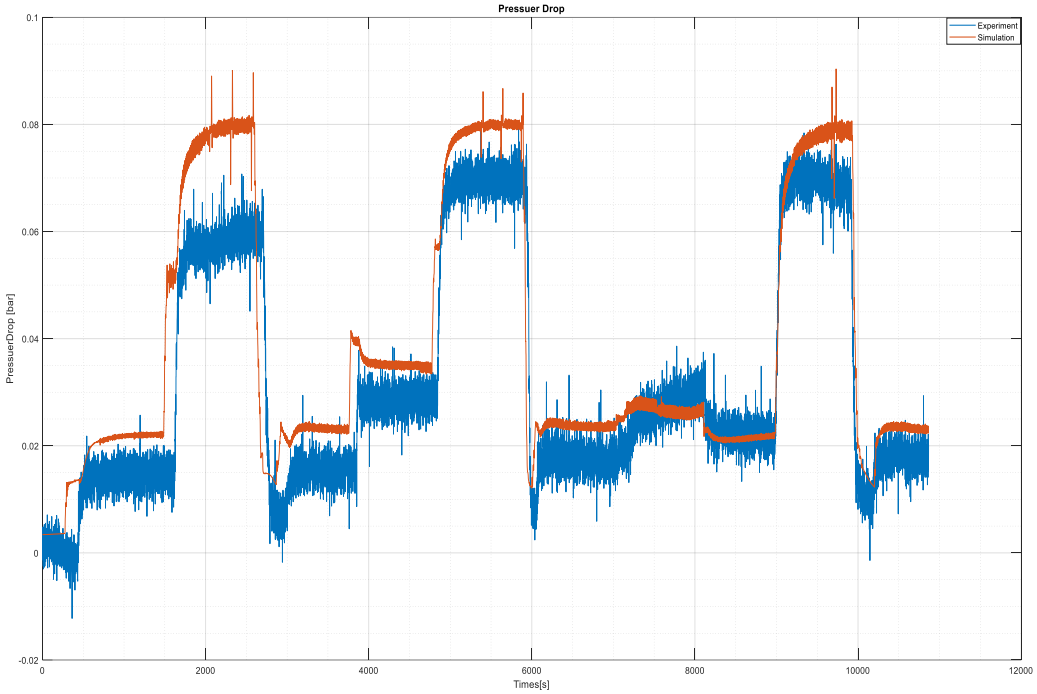

Figure 44: The result for pressure drops when wall permeability equal to 6e-14.

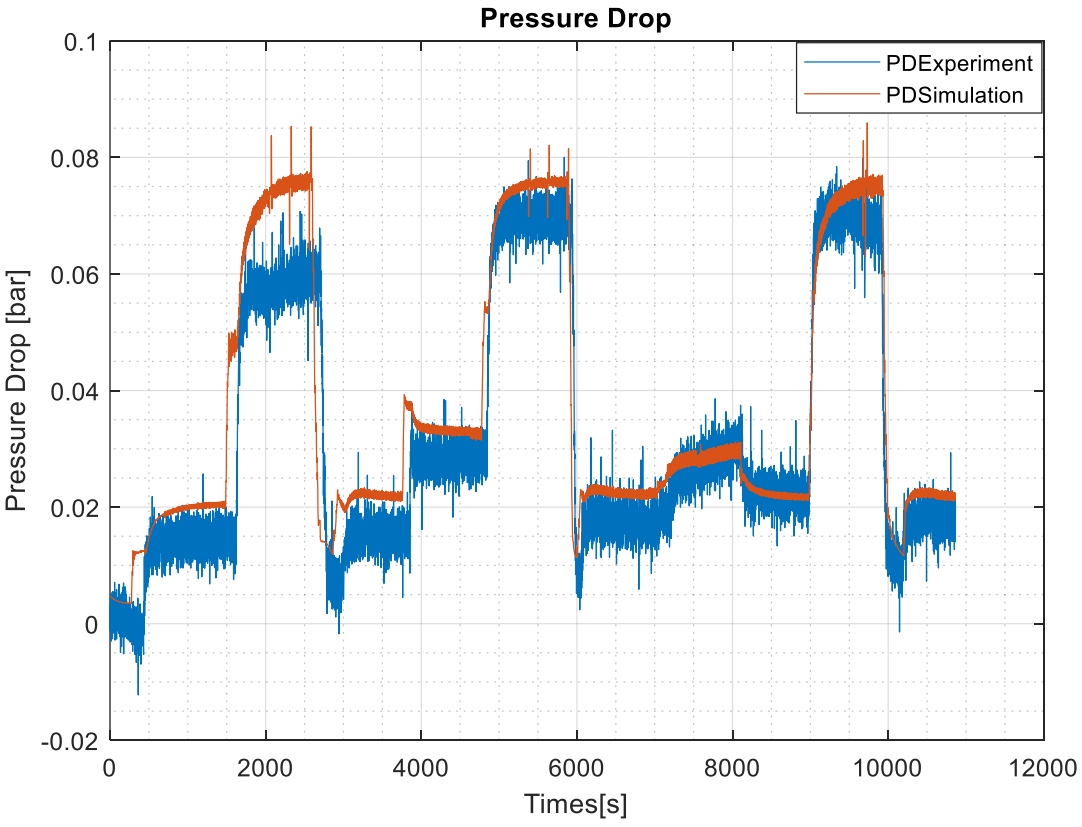

Figure 45: The result for pressure drops when wall permeability equal to 2e-14.

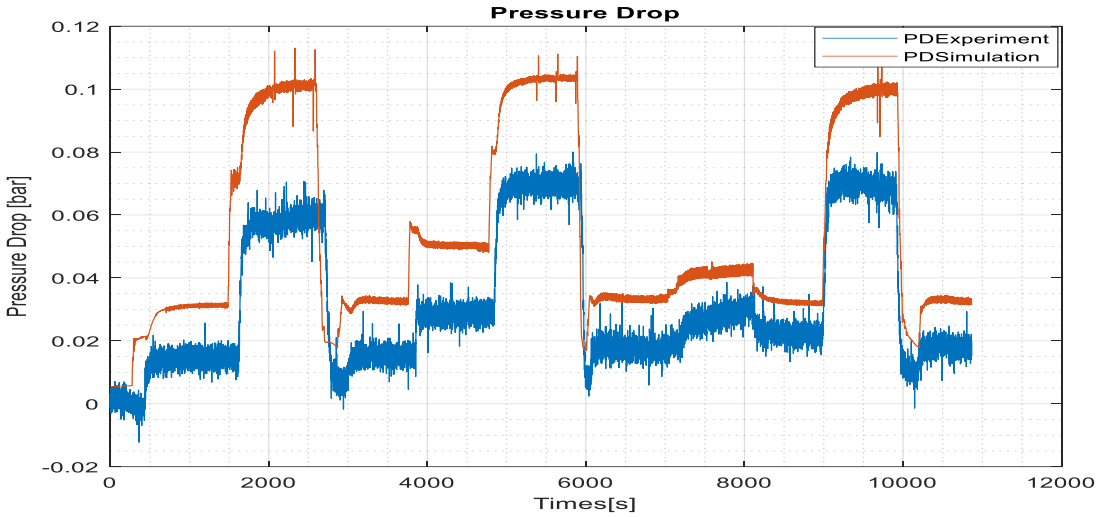

Figure 46: The result for pressure drops when wall permeability equal to [2e-15, 6e-15]

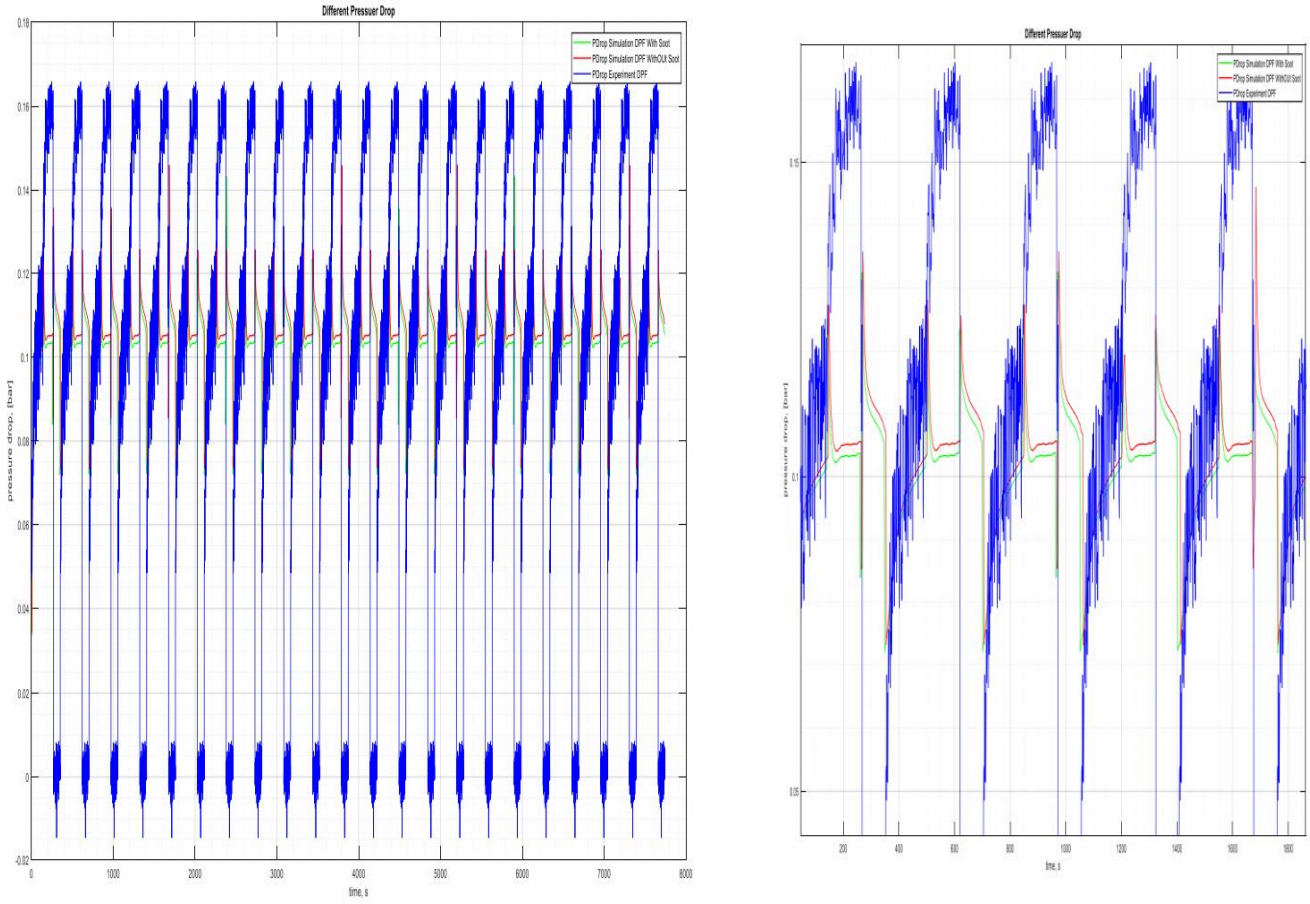

Figure 47: The result for pressure drops for test DOC-DPF model with test cycle [A25-A75-B50-C50] and wall permeability 5e-13. Green line pressure drop simulation with soot, red line pressure drops without soot, blue line pressure drop experiment.

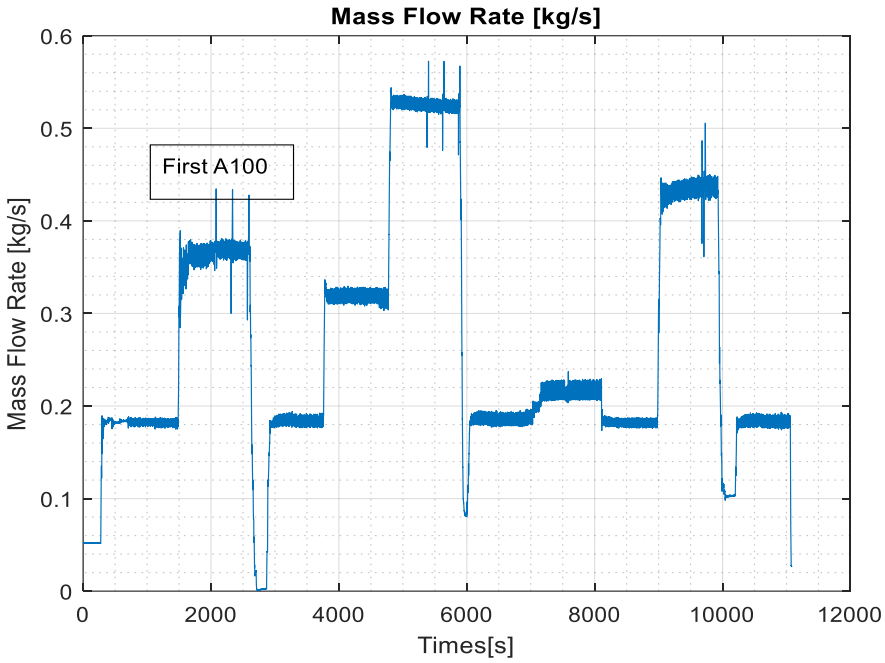

Figure 48: Mass flow rate after decrease with 2.5% for first A100.

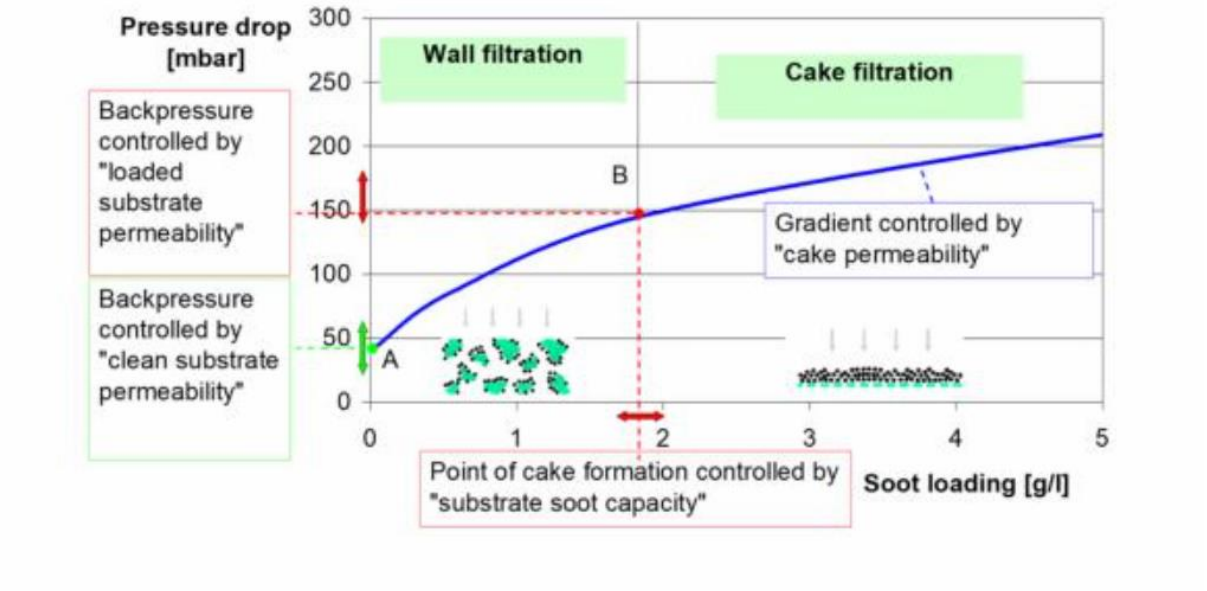

Figure 49: Pressure drop parameters calibration, where the increase in A value led to better wall filtration and this project the focus was to optimizing wall filtration

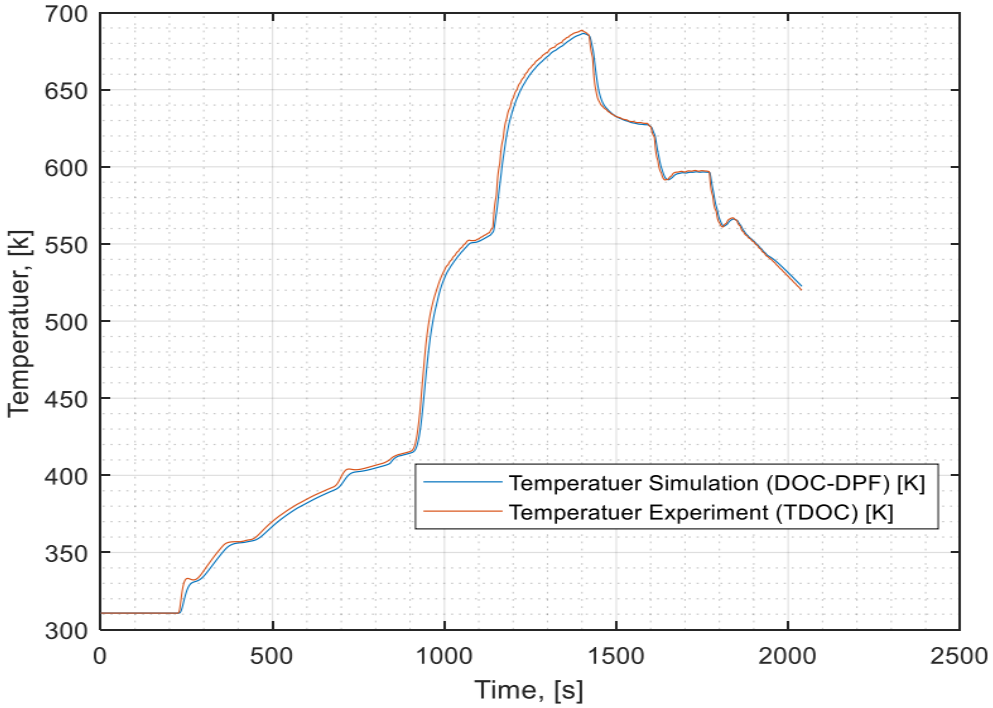

Figure 50: Temperature result for the test model shown the result for temperature simulation (DOC-DPF) versus temperature experiment (DOC-Temp_In).

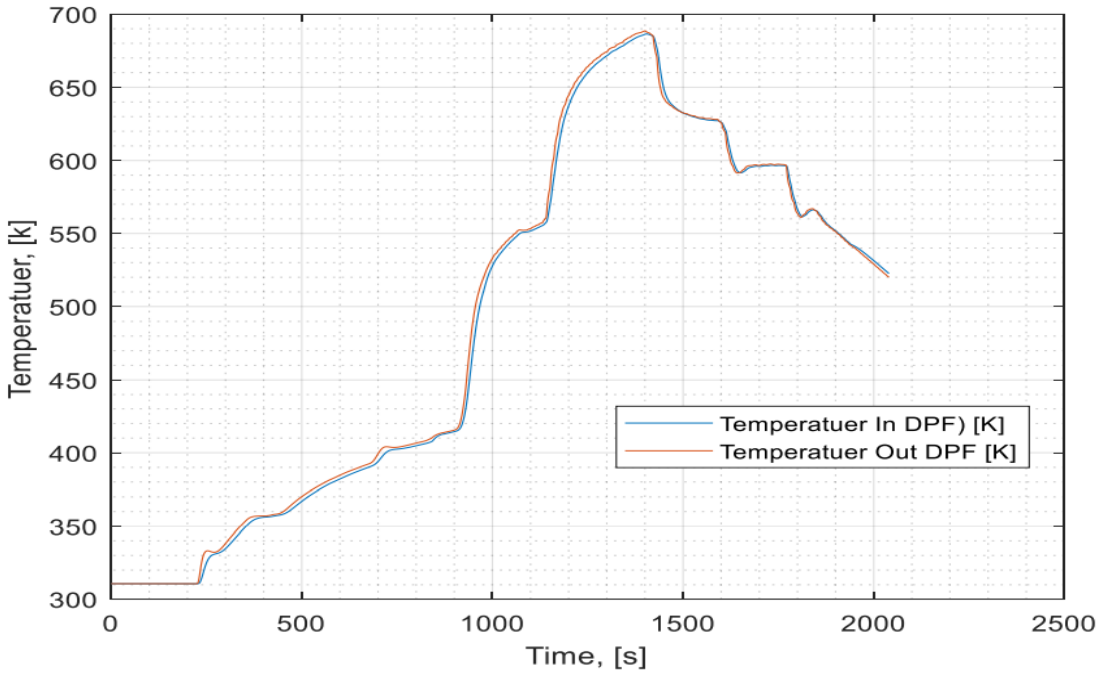

Figure 51: Temperature result for the test model shown the result for temperature simulation (DPF In) versus temperature experiment (DPF Out).

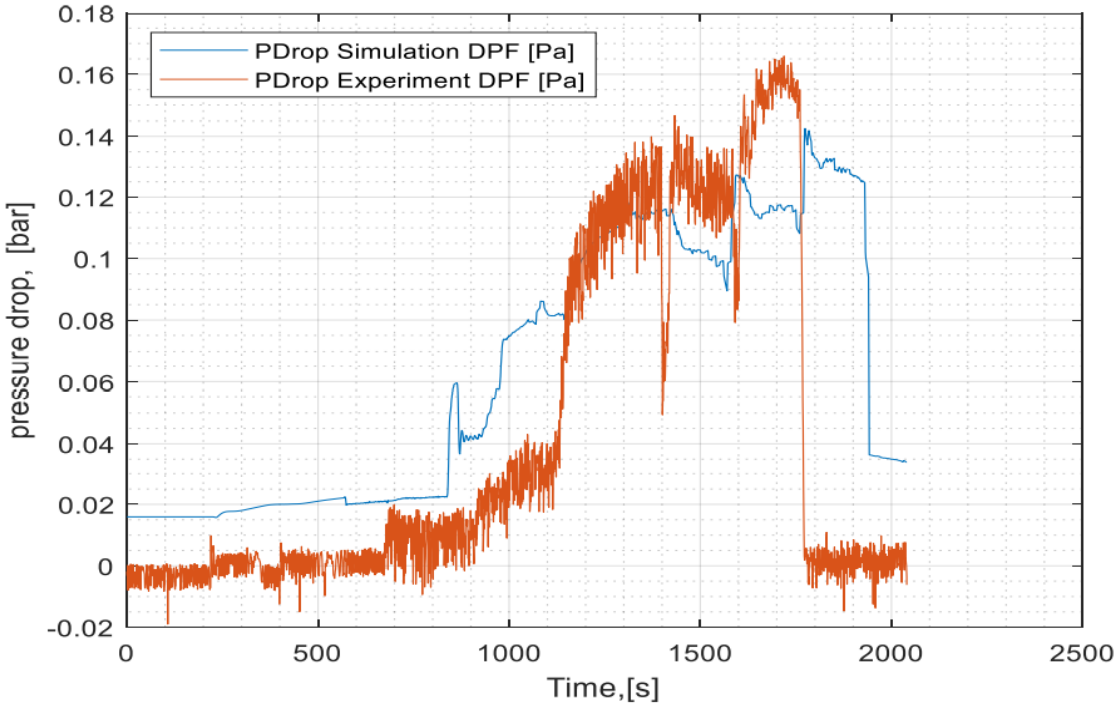

Figure 52: The result for pressure drops (simulation versus experiment) for test model without change parameters. From the figure it is clear the difference in the results, which leads to not understanding the loading of soot correctly.

Appendix 3: User guide for managing data and the important aspect model design (Axisuite)

In this appendix, readers will be given instructions for important steps in the method of designing a form and entering data.

- All data collected from the experiment must be converted to a format compatible with the program *Axisuite* (. *xlsx) especially the vision file, which contains basic information, mass flow rate.

- Before entering the required input data, it must be processed in the *MATLAB* to filter soot concentrations, for example. Most of the time, the data from the experiment contains unwanted data such as information that was collected before the engine reached the stationary stage, so it must be filtered before it is used as input data.

- Calculate all input data for the NO2, NO, O2 concentrations by using the *MATLAB*, the equations mentioned in the section 4.2.2 and 4.2.3.

- When designing the model using a *Axisuite* software, the following matters that have an impact on the simulation results must be considered:

- Soot distribution: In the absence of particle size data, the soot distribution method (realistic) and the normal of the distribution method must be considered.

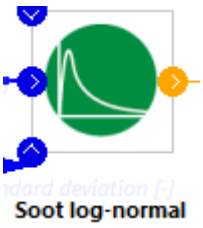

- Using the same dimensions and materials used in the model in accordance with what is used in the experiment. The results differ according to the materials used inside the catalyst, due to the different properties of the materials, for example, the endurance temperature. (Component manger)

- Adjust all soot reaction to match the studied condition (Soot, Ash), the soot properties should be selected to meet the Euro emission class (I, IV, VI, Etc.).

- Choosing the accuracy of the network has a great influence on the simulation results. It is better to choose 3D to get accurate results (simulation time becomes longer).

- Adjusting the reaction rate in a way that helps a higher oxidation of soot by oneself, the method used in the section 5.2.1.

CHALMERS
UNIVERSITY OF TECHNOLOGY